CHALMERS

WLAN MIMO Terminal Test in Reverberation Chamber

NATALIA OLANO

Antenna Group
Department of Signals and Systems
Chalmers University of Technology
Gothenburg, Sweden, 2008

WLAN MIMO TERMINAL TEST IN REVERBERATION CHAMBER

Master Thesis Report

By Natalia Olano

Supervisors: Charlie Orlenius (Bluetest AB)
Katsunori Ishimiya (Sony Ericsson AB)
Zhinong Ying (Sony Ericsson AB)

Examiner: Prof. Per-Simon Kildal

Sony Ericsson Mobile Communications AB
Lund, Sweden

Bluetest AB
Göteborg, Sweden

Antenna Group
Chalmers University of Technology
Gothenburg, Sweden
October 2007 – April 2008

Abstract

Convergence of portable consumer electronics, telecommunications, networking and multimedia entertainment platforms is nowadays a reality that demands increasing data rates and better coverage of wireless networks. In this context, MIMO antenna systems have been developed to raise the throughput without an increase in occupied bandwidth or modulation complexity and to improve coverage with no line of sight. Such advanced systems include complicated signal processing algorithms that have to drive very elaborated communication protocols and make the RF specifications on the transmitters and receivers more stringent. There is a need for a test method that provides verification of the full system, with the antennas included, proving to be reliable and to yield results that resemble the real world performance.

This Master Thesis report presents a method to characterize full system MIMO WLAN performance in terms of link throughput by using a reverberation chamber to provide Rayleigh fading conditions resembling the multipath indoor environment in which WLAN most usually has to perform together with shielding from interference.

Preface

This report is a Master Thesis work for the completion of the MSc degree in Telecommunication Systems and Networks Engineering at Universidad Carlos III de Madrid. It has been carried out in the framework of an agreement with Chalmers University of Technology after a previous exchange year of taking courses in Chalmers inside the European Erasmus program.

The research project was proposed by Sony Ericsson and Bluetest within the Chalmers Antenna Systems Excellence centre (CHASE) in the "Measurement Techniques for MIMO and Wideband Systems" program.

The examiner for the Master Thesis has been Per-Simon Kildal at the Antenna Group in Chalmers, whereas the supervisors were Charlie Orlenius from Bluetest and Katsunori Ishimiya and Zhinong Ying from Sony Ericsson. Financial support for the project and test units has been supplied by Sony Ericsson.

The work, including measurements in the reverberation chamber, was carried out in the Bluetest High Performance chamber located in Bluetest's office in Gothenburg except for the RF characterization of the router that was performed with the instruments in the laboratory of the Antenna Group in Chalmers.

The post-processing of reference measurements for the time-domain characterization of the chamber was done by Chen Xiaoming, Ph. D. student at the Antenna Group in Chalmers.

The timeline of the project was 1 October 2007 to 22 April 2008.

Acknowledgements

My deepest gratitude to Per-Simon Kildal, Charlie Orlenius and Mats Andersson in the Antenna Group and Bluetest for including me in this project, giving me a wonderful opportunity, and also for sharing with me their views and knowledge. Special thanks go as well to Thomas Bolin, Katsunori Ishimiya and Zhinong Ying from Sony Ericsson, who also contributed with their experience and their helpful attitude. It has been a pleasure to belong to such a collaborative and highly competent environment and to participate in an initiative like CHASE. I will always take the approach to work that I have learnt here with me.

Thanks as well to Jan Sjögren, application engineer from Agilent, who helped me with the validation and troubleshooting of the measurement setup in the Agilent N4010 with the Agilent Graphical Interface 89601A.

I would like to mention Daniel Segovia, my exchange coordinator and thesis tutor in University Carlos III of Madrid for his help and Eva Rajo, also from Carlos III and whom I surprisingly met in Sweden, for her encouragement and her closeness.

Thanks to my parents and my whole family for their love and support. To my mother for teaching me what it is to be a woman in science, to my father for his daily emails, to my grandmother Concha for her example of strength in the hardest times and to my grandfather Poli, who has always liked to inspire curiosity for everything in his grand children.

I want to mention Stefan as well, because he has taken up the task of making me smile every day since we met and he has always succeeded, even from far away. To acknowledge my friends: Miriam, both Ana's, Virginia… for so many hours of hard work in the university but also of laughs together, Lucía and Blanca for our long years of friendship and trust, Juan, for believing in me when there was so much to do left, both Laura's, Estela and everyone in Högsbogatan, with whom I have gone through good and hard times in Sweden, for their warmth when we were away from home, and to my colleagues and friends in Bluetest and the Antenna Group, Magnus, Elena, Daniel, Antonio, Chen, Adeel, Nima… because not only they have helped me throughout this work but we have also shared great moments.

Finally, if you are reading this and feel you should be included, you are probably right. Please forgive me because there were many people I wanted to thank now that I have finished my studies and it was easy to miss one or even a couple of them ;) Share with me the moment of happiness of reaching an objective pursued for long years!

Table of contents

Chapter 1: Introduction 1
Chapter 2: Multiple Input Multiple Output 3
2.1 Spatial multiplexing 4
2.2 Transmitter beamforming 5
2.3 Diversity 5
Chapter 3: WLAN 7
3.1 Introduction 7
3.2 WLAN HT PHY 7
3.2.1 Transmitter block diagram 8
3.2.2 Orthogonal Frequency Division Multiplexing 11
3.2.3 Guard Interval 12
3.2.4 MIMO channel estimation process 13
3.2.5 Link adaptation 14
3.2.6 Transmitter beamforming 15
3.2.7 Antenna selection 15
3.2.8 Space-time block coding 15
3.3 WLAN HT MAC 16
3.3.1 Aggregation 16
3.3.2 Block Acknowledgement 18
3.3.3 Reduced Interframe Space 18
Chapter 4: State of the art on measurements of WLAN devices 21
4.1 RF performance 21
4.1.1 IEEE 21
4.1.2 CTIA 22
4.2 Throughput Benchmarking 23
4.2.1 Field tests 24
4.2.2 Measurements in shielded chambers 24
4.2.3 Isolated Cabled Test Beds 24
4.2.4 Channel emulators 25
Chapter 5: RF Characterization of the AP 29
5.1 Description of the measurement instrument 29
5.2 Definition of parameters in the transmitter test 30
5.2.1 Transmit power 30
5.2.2 Transmit spectral mask test 30
5.2.3 Transmit cross-power and channel isolation 30
5.2.4 Transmitter Error Vector Magnitude 31
5.3 Measurement setup 32
5.4 Results 34
5.4.1 Frame format and MCS implementation in the DUT 35
5.4.2 Spatial mapping implementation 36
Chapter 6: Reverberation Chamber 37
6.1 Introduction 37
6.2 Description of the fading in the chamber 38
6.3 Calibration of the environment in the chamber 38
6.3.1 Coherence bandwidth 39
6.3.2 Coherence time 39

Chapter 7: Throughput test in the reverberation chamber 41
7.1 Background 41
7.1.1 Transport layer protocol and parameters 41
7.1.2 Wireless security algorithms 42
7.1.3 Quality of service 42
7.1.4 MAC frame size 42
7.1.5 PHY configurations 42
7.1.6 Channel characteristics 42
7.1.7 Distance 43
7.1.8 Interference 43
7.2 Throughput measurement setup 43
7.2.1 Basic setup 43
7.2.2 Problems and modifications of the basic setup 45
7.2.3 Improved setup 47
7.2.4 Problems and suggested modifications of the improved setup 48
7.3 Results acquired in the basic setup 48
7.3.1 Statistical characteristics of the measurement 48
7.3.2 Comparison of WLAN standards 49
7.4 Results acquired in the improved setup 50
7.4.1 Average Receive Signal Strength Indicator 50
7.4.2 Downlink throughput of different MIMO antenna configurations 52
7.4.3 Unbalanced channel cases 53
7.4.4 Downlink throughput of different MIMO antennas 55
7.4.5 Uplink throughput of different MIMO antenna configurations 56
Chapter 8: Final discussion 59
References 63
Appendix I: Certification entities 65
Appendix II: Router control web interface 67
Appendix III: Measured data for the statistical approach 69

List of figures

Figure 1: Signal intensity map of an indoor location 3
Figure 2: Average powers of normalized 4x4 MIMO measured channel responses 4
Figure 3: Transmitter block diagram for the HT Greenfield format packet and HT portion of the mixed format packet except HT signal field 8
Figure 4: Data scrambler 8
Figure 5: Direct mapping transmitter and receiver schematic 10
Figure 6: Spatial expansion transmitter 10
Figure 7: Spatial beamforming transmitter 10
Figure 8: Single OFDM carrier in time and frequency to the left and OFDM spectrum to the right 11
Figure 9: Ideal OFDM transmitter block diagram 12
Figure 10: Recovery of an OFDM symbol 12
Figure 11: ISI due to multipath propagation and periodic extension solution 13
Figure 12: WLAN PHY protocol data unit in HT mixed format 14
Figure 13: OFDM symbol manipulation used in space time block coding 16
Figure 14: 802.11 MAC protocol overhead 16
Figure 15: 802.11n Frame aggregation 17
Figure 16: Architecture of the MAC and PHY layers with indications of where MSDUs and MPDUs are originated 17
Figure 17: MAC Service Data Units Aggregation 18
Figure 18: MAC Protocol Data Units Aggregation 18
Figure 19: Three iterations of an 802.11a throughput measurement over two minutes in an isolated test bed to the left and under uncontrolled fading and interference to the right 25
Figure 20: Diagram of a 4x4 channel emulator 25
Figure 21: Block diagram of the switch matrix approach for MIMO testing 29
Figure 22: Sequential capture process of a two-channel MIMO signal 30
Figure 23: Comparison of the channel response of direct-mapped (above) and spatially-mapped devices (below) 31
Figure 24: Definition of Error Vector Magnitude 32
Figure 25: Maximum EVM values in the 802.11n draft standard 32
Figure 26: N4010 Measurement setup 34
Figure 27: Implementation of the MCS in the router 35
Figure 28: Router frequency response per channel and spatial stream 36
Figure 29: Bluetest High Precision Chamber 37
Figure 30: Distribution of angles of incidence in the reverberation chamber in 0.8m x 1.1m x 1m chamber (GSM 900 band) 38
Figure 31: Scheme of the basic measurement setup 44
Figure 32: Pictures of the basic measurement setup 44
Figure 33: Power filters in the N-connectors 46
Figure 34: Improved setup software graphical interface 46
Figure 35: Improved setup layout 47
Figure 36: Repeatability of the measurement in the basic setup 49
Figure 37: Comparison of WLAN standards 50
Figure 38: Antenna numbering in the router 50
Figure 39: RSSI at the USB adapter in the different MIMO antenna configurations 51
Figure 40: RSSI at the USB adapter per MIMO antenna configuration 51

Figure 41: Downlink throughput of different MIMO antenna configurations 52
Figure 42: Comparison of MIMO antenna configurations in the basic setup..... 53
Figure 43: Downlink Throughput of Unbalanced Channel Cases 54
Figure 44: Throughput as a function of the attenuation in XXO configuration 54
Figure 45: Dielectric resonator antenna prototype with PWB 55
Figure 46: Downlink throughput of MIMO antenna sets 56
Figure 47: Comparison DRA and dipole set in the basic setup 56
Figure 48: Uplink throughput of different MIMO antenna configurations 57
Figure 49: Wireless Network Settings Menu 67
Figure 50: Advanced Wireless Settings 68

List of tables

Table 1: Minimum receiver sensitivity in the 802.11n third draft of the standard 22
Table 2: 802.11n TGn channel models 26
Table 3: Measurement of the average throughput of an 802.11n device as a function of the large scale path loss for different channel models in a fading simulator 26
Table 4: Statistical characteristics of the measurement 49

List of equations

Equation 1: 2x2 MIMO channel matrix 4
Equation 2: Instantaneous maximum capacity of the MIMO system as a function of the channel matrix coefficients 5
Equation 3: Instantaneous maximum capacity of the MIMO system as a function of the channel matrix singular values 5
Equation 4: Definition of frequency autocorrelation coefficient 39

Abbreviations and acronyms

AP	Access Point
BPSK	Binary Phase Shift Keying
CTIA	Cellular Telecommunications and Internet Association
DUT	Device Under Test
FFT	Fast Fourier Transform
IFFT	Inverse Fast Fourier Transform
HT	High Throughput
ICI	Inter Carrier Interference
IEEE	Institute of Electrical and Electronics Engineers
ISI	Inter Symbol Interference
MAC	Medium Access Control
MCS	Modulation Coding Scheme
MIMO	Multiple Input Multiple Output
MPDU	MAC Protocol Data Unit
MSDU	MAC Service Data Unit
OFDM	Orthogonal Frequency Division Multiplexing
OTA	Over The Air
PHY	Physical Layer
PPDU	PHY Protocol Data Unit
QAM	Quadrature Amplitude Modulation
QPSK	Quadrature Phase Shift Keying
RF	Radio Frequency
STA	Station
TIS	Total Isotropic Sensitivity
TRP	Total Radiated Power
Wi-Fi	Wireless Fidelity
WEP	Wired Equivalent Privacy
WLAN	Wireless Local Area Networks
WPA	Wi-Fi Protected Access

Chapter 1: Introduction

Next generation wireless communication systems such as WLAN (Wireless Local Area Networks) and WiMAX (Worldwide Interoperability for Microwave Access) rely on MIMO (Multiple Input Multiple Output) technologies to provide advanced services with high performance demands. It has been proven that they offer a significant enhancement in throughput and coverage, but there has not been a repeatable testing methodology that covered the whole system to check the real quality of the link in a normal environment of operation.

The present study deals with the application of the reverberation chamber techniques for testing WLAN MIMO devices. The fading environment inside the reverberation chamber follows a Rayleigh distribution, with large resemblance to indoor or urban environments where most commonly WLAN operation takes place and the Bluetest High Precision chamber has enough space to place all the components of the WLAN link to test inside a 100dB shield to provide proper isolation from interference that, as will be explained later, is a key limiting factor in the performance of these systems.

This report is divided in eight chapters. After this first introductory chapter, chapter 2 clarifies the terminology for MIMO systems used during the report. Chapter 3 contains a study of the 802.11n communication protocol characteristics provided to understand the measurement results. A thorough research on the state of the art of measurements of WLAN devices and especially on the existing WLAN throughput measurements is provided in chapter 4. In chapter 5 are described the most important RF parameters of a MIMO WLAN transmitter, the test equipment to be used in RF measurements in WLAN and a measurement setup with the N4010 Agilent Wireless Connectivity Test Set. Chapter 6 provides a short overview of the existing reverberation chamber techniques, together with the characterization of the transmission channel in the reverberation chamber performed over a reference measurement. Finally, the throughput measurement in the reverberation chamber is discussed in chapter 7, with the comparison of two different setups in layout and software and the exposition of measurement results to explore the capabilities of the method. The final discussion compiles the conclusions on the results and suggests improvements to the measurement setups for future work.

Chapter 2: Multiple Input Multiple Output

WLAN devices suffer strong fading due to multipath propagation, especially since they are mostly used in urban and indoor environments with plenty of scattering. The figure below, from [1], shows a map of the differences in field strength for a simple square room with a metal desk in the lower left and an open doorway at the top right. It is a static snapshot that would be altered if stations and objects in the environment would move and shows the high variability of field strength with the position.

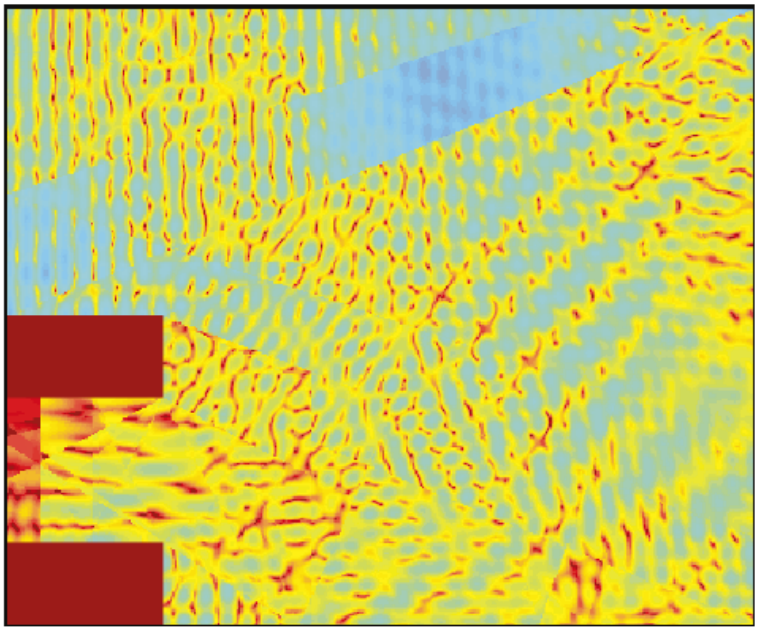

Figure 1: Signal intensity map of an indoor location

MIMO techniques benefit from the characteristics of the radio multipath transmission being strongly dependent on the position of the antenna to increase the capacity of the radiofrequency link, its coverage and also its robustness. This is done by using three main different approaches: *spatial multiplexing*, *beamforming* and d*iversity*. This chapter gives definitions of these concepts in the context of WLAN.

2.1 Spatial multiplexing

The signals received by a set of spatially separated of antennas when a number of spatially separated antennas transmit at the same time are described by a set of linear equations if the bandwidth is small enough so that the channel response can be represented by a constant [2].

$$\begin{bmatrix} T_1 \\ T_2 \end{bmatrix} = \begin{bmatrix} h_{11} & h_{12} \\ h_{21} & h_{22} \end{bmatrix} \begin{bmatrix} R_1 \\ R_2 \end{bmatrix}$$

where T_1, T_2 are the signals transmitted by transmitting antennas 1 and 2
R_1, R_2 are the signals transmitted by receiving antennas 1 and 2
$\{ h_{ij} \}$ are the channel coefficients

Equation 1: 2x2 MIMO channel matrix

This means that the different transmitted signals can be extracted from the received ones via proper digital signal processing. The strategy of sending radiofrequency data streams in parallel is called *spatial multiplexing* and offers the possibility to increase the capacity of the RF link as will be shown later.

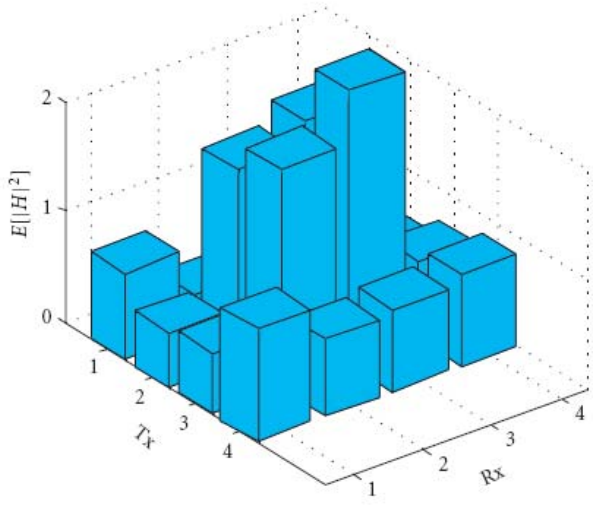

Figure 2: Average powers of normalized 4x4 MIMO measured channel responses

The figure above shows how the various spatial channels may strongly differ in their response. Besides, if an antenna is moved even a quarter of a wavelength, different coefficients apply for the equation that defines the new path.

The channel capacity is the number of bits per second and Hz of bandwidth that can be transmitted through a radio channel. The instantaneous maximum capacity of a MIMO system, derived from the expression of the channel capacity in Shannon´s Theorem follows equation 2.

$$C_{MIMO} = \log_2\left(\det\left(I_{MXN} + \frac{SNR}{N} H_{MXN} \cdot H^*_{MXN}\right)\right)$$

where N is the number of transmitting antennas
M is the number of receiving antennas
H_{MXN} is the radio channel matrix

Equation 2: Instantaneous maximum capacity of the MIMO system as a function of the channel matrix coefficients

Mathematical manipulation of equation 2 yields equation 3, where the summation sign shows the capacity increasing linearly with the number of transmitter-receiver chains.

$$C_{MIMO} = \sum_{i=1}^{L} \log_2\left(1 + \frac{SNR}{N}\sigma_i^2(H)\right)$$

where N is the number of transmitting antennas
L is the number of independent transmitter-receiver chains
$\sigma_i^2(H)$ are the singular values of the radio channel matrix, H

Equation 3: Instantaneous maximum capacity of the MIMO system as a function of the channel matrix singular values

Therefore, spatial multiplexing introduces a gain in capacity even when the transmitted power needs to be divided amongst the transmitters, because the degradation of the SNR resulting from the power decrease causes a loss in capacity only on a logarithmic basis and the increase of capacity derived of sending several data streams in parallel is linear.

2.2 Transmitter beamforming

Beamforming consists on the application of different phase rotations to the signals at each transmitting antenna port so that the reception is improved in the other end of the link. By doing this it is possible to reduce the number of black spots inside a coverage area. Note that in this MIMO context the "beam" applies to a particular spatial stream, not a beam in the phased-array sense.

The coefficients used for this purpose are known as steering vectors or Q matrix. They are calculated based on some knowledge of the channel acquired during a system training period. Sections 3.2.4 and 3.2.6 explain the procedures defined in the standard for channel estimation and beamforming.

2.3 Diversity

Diversity improves the robustness of the transmission by either transmitting or receiving multiple copies of the same signal. Transmitter diversity is regarded in the standard and implemented via Spatial Time Block Coding.

Chapter 3: WLAN

3.1 Introduction

WLAN specifications are comprised in the IEEE 802.11 standard papers, [1]. Those include medium access control (MAC) and physical layer (PHY) descriptions that were later extended by standards 802.11b[3], a [4], g [5] and finally n [6], which is currently under development and builds on the previous standards basically by adding MIMO to the PHY and packet aggregation plus reduced interframe spacing to the MAC.

Despite the fact that there are already many products on the market based on Draft 2.0 of 802.11n standard, and the third specification draft was published in November 2007, the amendment will still have to wait until July 2009 regarding to the Official IEEE 802.11 Working Group Project Timelines.

The aim of the 802.11n standard is to provide PHY and MAC features to support a throughput of 100 Mbps and greater in the downlink, measured at the MAC data service access point. Stations (STA) and access points (AP) with this capability are known as High Throughput (HT) and support MIMO operation, transmit beamforming, spatial time block coding, low density parity check encoding and antenna selection in the PHY. Their MAC features include frame aggregation, block frame acknowledgement, power save multi poll operation and reverse direction. The transmission bandwidth can be either 20 or 40 MHz and the system can operate both in the 2.4 GHz and 5 GHz band.

The standard offers three different configurations to provide compatibility with previous amendments: non-HT, HT mixed, and HT greenfield. Each of these configurations works with a different frame format. The HT PHY supports non-HT operation in the 2.4 GHz band as defined by standard 802.11b [3] and g [5] clauses 18 and 19, and in the 5 GHz band as defined by 802.11a [4] clause 17. Protection mechanisms supporting coexistence with non-HT STAs and non-HT APs are also specified.

The WLAN section of this report focuses on the PHY and MAC layer features of the 802.11n standard that are important for understanding the phenomena occurring during the measurements in reverberation chamber.

3.2 WLAN HT PHY

The HT PHY is based on the orthogonal frequency division multiplexing (OFDM) PHY defined in 802.11a [4] clause 17, with extensibility up to 4 spatial streams, operating in 20MHz bandwidth. Additionally, transmission using 1 to 4 spatial streams is defined for operation in 40MHz bandwidth. These features are theoretically capable of supporting data rates up to 600 Mbps with 4 spatial streams and 40 MHz bandwidth. However, mandatory implementation comprises only one and two spatial streams at an AP and one spatial stream at a STA, both with 20 MHz bandwidth. The rest of the configurations are optional. In fact, the majority of Draft 2

certified devices up to date support 2 spatial streams, configuration that yields maximum link rates of 144 Mbps for 20 MHz operation and 300 Mbps for 40 MHz.

3.2.1 Transmitter block diagram

The transmitter is composed of the following blocks, explained below in detail:

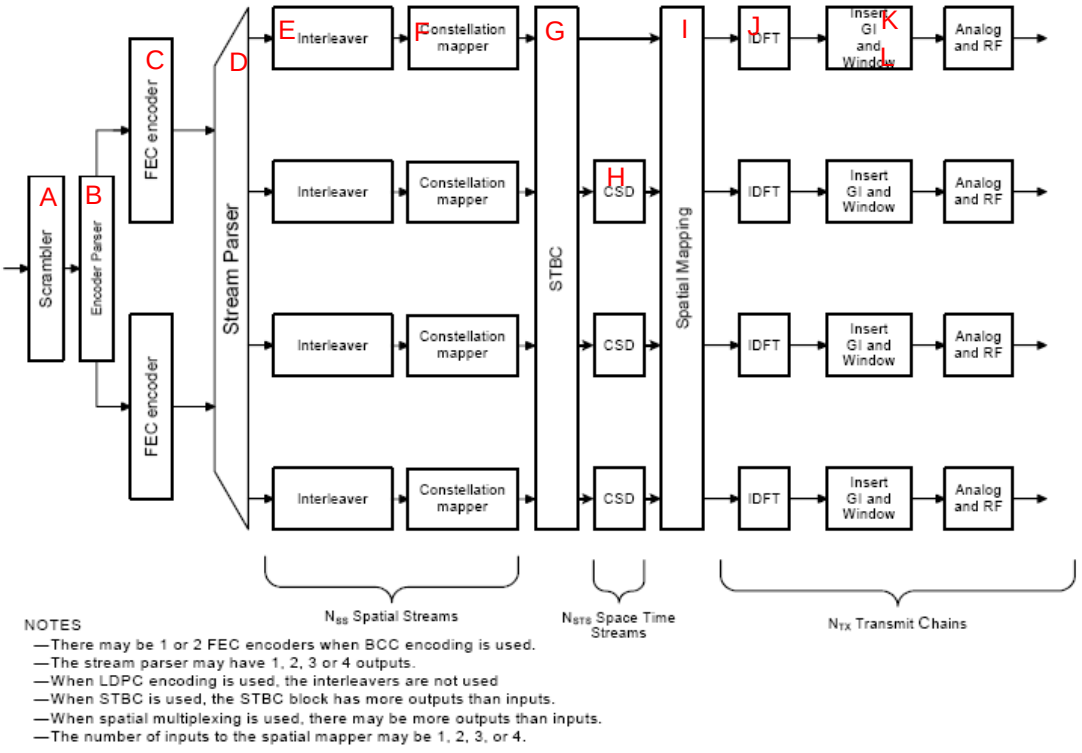

Figure 3: Transmitter block diagram for the HT Greenfield format packet and HT portion of the mixed format packet except HT signal field

A. *Scrambler*: Scrambles the data to reduce the probability of long sequences of zeros or ones. The full DATA field of the frame shall be scrambled with a 127 bit frame-synchronous scrambler using the generator polynomial $S(x)=x^7+x^4+1$ as illustrated below:

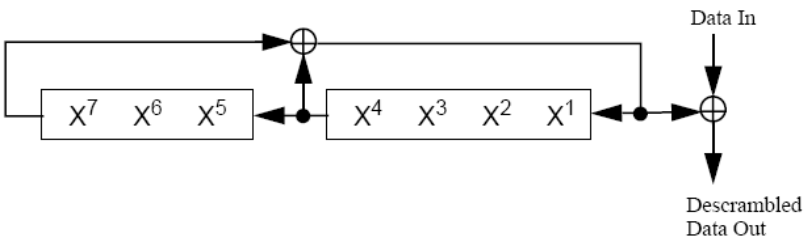

Figure 4: Data scrambler

For more information see [4] 17.3.5.4.

B. *Encoder parser:* When Binary Convolutional Coding is used, demultiplexes the scrambled bits among the number of encoders in a round robin manner, see [4] 20.3.10.5 for more details. A single forward error correction encoder is always used when Low Density Parity Check coding is chosen and in that case parsing becomes unnecessary.

C. *Forward error correction encoders*: The data field is encoded using either the binary convolutional code defined in [4] 17.3.5.5 and [6] 20.3.10.5, or the low-density parity check code defined in [6] 20.3.10.6. Low-density parity check codes are can be used in the HT system as a high-performance error correcting code, instead of the convolutional code. However, their implementation is optional.

D. *Stream parser*: Divides the outputs of the encoders into the spatial streams that are sent to different interleaver and mapping devices.

E. *Interleaver*: Changes the order of the bits in each spatial stream to prevent long sequences of adjacent noisy bits from entering the binary convolutional code decoder. Not used when low-density parity check is applied.

F. *Constellation mapper*: Maps the sequence of bits in each spatial stream to the constellation points in the complex plane. The HT PHY data subcarriers are modulated using binary phase shift keying (BPSK), quadrature phase shift keying (QPSK), 16-quadrature amplitude modulation (16-QAM), or 64-QAM and the mapping is done as defined in [4] 17.3.5.7

G. *Space time block encoder*: Transmitter diversity technique applicable only for asymmetric arrangements with a single antenna at the receiving end of the link. See 3.2.8.

H. *Cyclic shift insertion***:** Insertion of the cyclic shifts prevents unintentional phased array beamforming due to simultaneous transmission from different antennas and that could alter the antenna transmission pattern. This block may be placed before or after the IDFT.

I. *Spatial mapper*: Maps space-time streams to transmit chains. The transmitter may choose to rotate and/or scale the constellation mapper output vector (or the space-time block coder output, if applicable). This is useful in the following cases:

- When there are more transmit chains than space-time streams
- As part of (an optional) sounding packet
- As part of (an optional) calibration procedure
- When the packet is transmitted using an (optional) beamforming technique

Spatial mapping may be performed by using any of the following spatial mapping matrices. There exist many other alternatives, implementation is not restricted to these:

Direct mapping: Constellation points from each space-time stream are mapped directly one-to-one onto the transmit chains.

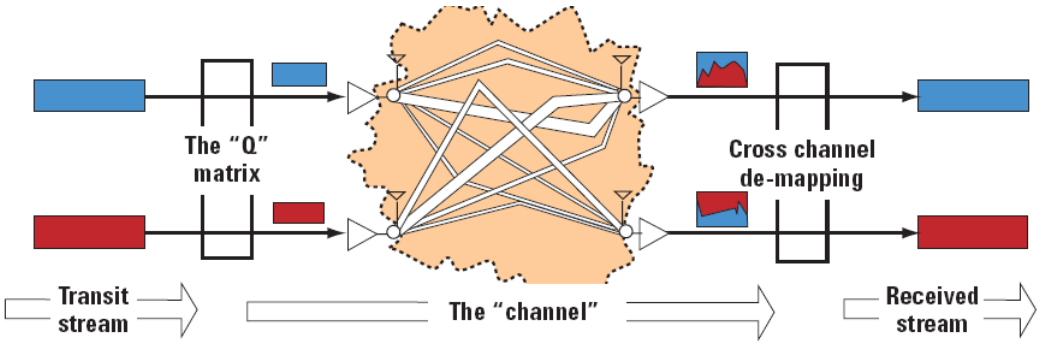

Figure 5: Direct mapping transmitter and receiver schematic

Spatial expansion: Vectors of constellation points from all the space-time streams are expanded via matrix multiplication to produce the input to all the transmit chains.

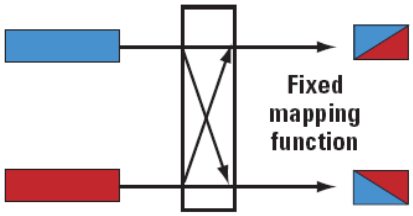

Figure 6: Spatial expansion transmitter

Beamforming: Each vector of constellation points from all the space time streams is multiplied by a matrix of steering vectors to produce the input to the transmit chains. The steering vectors are chosen to improve the reception in the receiver based on some knowledge of the channel.

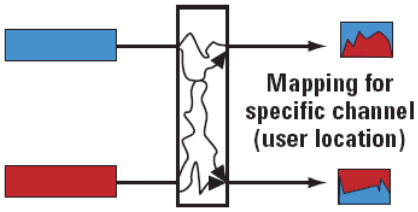

Figure 7: Spatial beamforming transmitter

More on beamforming can be found in 3.2.4 and [5] 20.3.10.10.1 and 20.3.11.

J. *Inverse discrete Fourier transform (IDFT)*: Converts a block of constellation points to a time domain block. More detail on OFDM modulation is provided in section 3.2.2.

K. *Guard interval insertion*: Prepends the symbol with a circular extension of itself. More detail on this mechanism in the OFDM section, 3.2.3.

L. *Windowing:* Optional smoothing of the edges of each symbol to increase spectral decay.

3.2.2 Orthogonal Frequency Division Multiplexing

The modulation format chosen for the standard is OFDM. It was first introduced in the 802.11a supplement to the IEEE WLAN standard and was proposed as a way of dealing with multipath, as mentioned in [2]. Most of the pictures in this section, as well as many of the explanations were taken from [7].

In a fading environment the symbol time cannot be shorter than the delay spread of the multipath channel because the transmission would suffer Inter Symbol Interference (ISI). Therefore, there is a limit to the achievable bandwidth using a single carrier modulation. Multi-carrier modulation formats are able to increase the available bandwidth by increasing the symbol interval over the delay spread and using a number of carriers. Each subcarrier is modulated with a conventional modulation scheme at a low symbol rate, maintaining data rates similar to conventional single carrier modulation schemes in the same bandwidth. This eliminates ISI and allows compensating for multipath effects with a simple equalizer.

OFDM uses sinusoid carriers. In a given period, the sinusoids will be orthogonal provided there is an integer number of cycles. That way Inter Carrier Interference (ICI) is eliminated and intercarrier guard bands are not required, what results in very high spectral efficiency.

Another advantage of the use of sinusoid carriers is that it allows for efficient modulator and demodulator implementation by means of the Fast Fourier Transform (FFT) algorithm, which today can be very efficiently calculated thanks to the advances in digital signal processing.

The two most important RF problems with OFDM are amplification, due to a high peak-to-average power ratio in comparison with other modulation formats and tight frequency synchronization requirements on accuracy and stability. With frequency deviation or phase noise, the sub-carriers shall no longer be orthogonal, causing ICI. Frequency offsets are typically caused by mismatched transmitter and receiver oscillators, non-linearities in amplification or by Doppler shift due to movement.

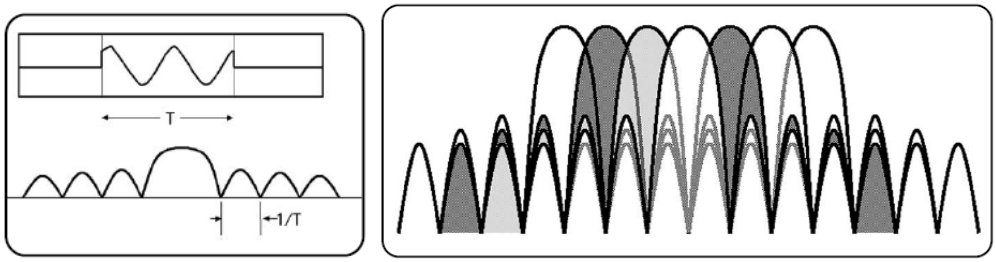

Figure 8: Single OFDM carrier in time and frequency to the left and OFDM spectrum to the right

Above is shown the way the different carriers add up to configure the OFDM spectrum. For a single carrier the transmitted pulse in the time domain is a sinusoid

multiplied by a pulse, which in the frequency domain, is a sinc function convolved with an impulse at the carrier frequency.

The magnitude and phase of each of the carriers are determined from the constellation symbol to be transmitted. As said before, the HT PHY data carriers can be modulated using several different modulation formats that can vary from spatial stream to spatial stream. Modulations formats available are BPSK, QPSK, 16-QAM, or 64-QAM and the mapping is done depending on the rate requested.

The complex number representing the symbol is transformed using the inverse FFT algorithm. This produces a set of time domain samples, which are then transmitted after being centred in the assigned frequency channel f_c as shown in the following figure.

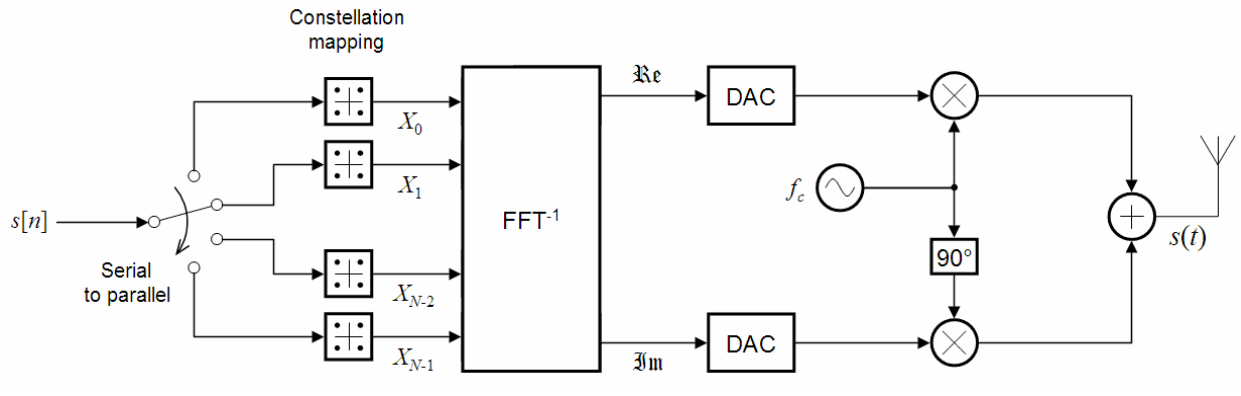

Figure 9: Ideal OFDM transmitter block diagram

In 20 MHz transmission the FFT size is 64, with 56 subcarriers used, four of them as pilots. For 40 MHz operation the FFT size is 128, of which 114 subcarriers are used with six as pilots. After the IFFT, all 64 or 128 time samples are transmitted. While a pulse is being transmitted, the next symbol is loaded into the FFT buffer.

3.2.3 Guard Interval

In the processing of a received OFDM signal the waveform is digitalized and converted back to a symbol using an FFT. This is illustrated in the following figure, where T_u refers to the meaningful part of the waveform:

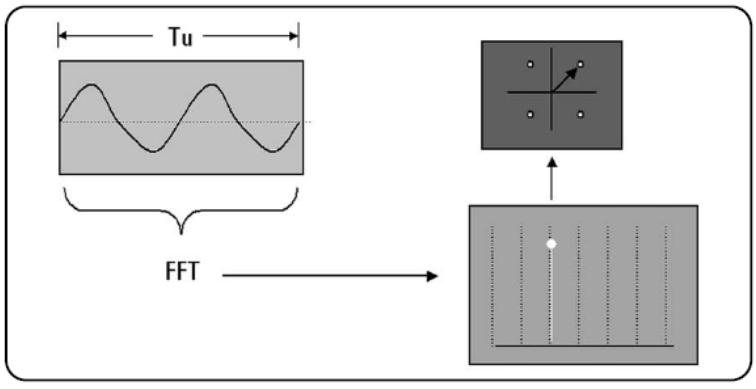

Figure 10: Recovery of an OFDM symbol

However, the OFDM signal above will not render a proper performance in multipath conditions. There will be some delay between the received signals from each of the reflected paths that will result on ISI in the receiver. To solve this problem a *cyclic extension* of the pulse is carried out. The last quarter of the pulse is copied and attached to the beginning of the burst. This is called the *guard interval,* T_g. The periodic nature of the FFT ensures the junction between the guard interval waveform and the start of the original burst will always be continuous. However, the waveform will still suffer from discontinuities at the junctions between adjacent symbols.

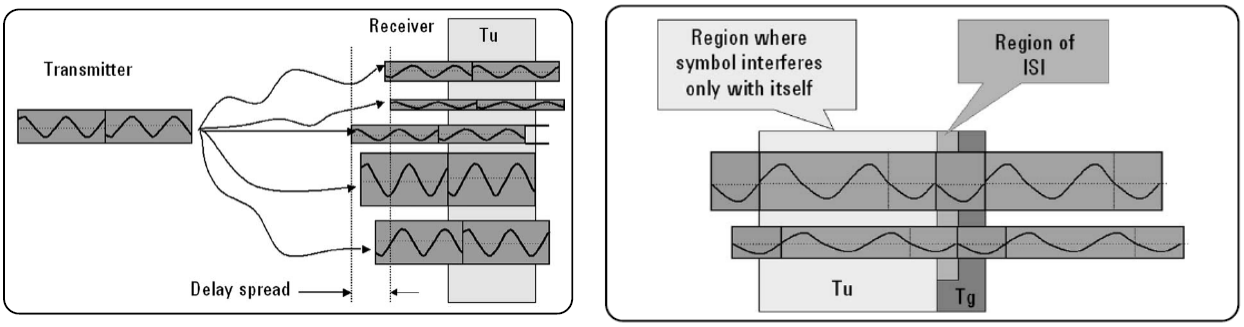

Figure 11: ISI due to multipath propagation and periodic extension solution

The previous figures illustrate how the addition of a guard interval removes ISI in the useful part of the signal. Each signal at the receptor has followed a different path and arrived at slightly different times. In the time interval denoted T_u, the signal will only interfere with itself. This amounts to no more than scaling and rotation of the symbol. In the guard interval region T_g the resulting signal has contributions from both symbols. If the guard interval is ignored in the receiver ISI does not degrade receiver performance. The guard interval needs to be longer than the delay spread, but not so long that throughput is lost.

The 802.11n operation allows for the guard interval to be selected depending on the severity of the multipath environment. Guard intervals of 802.11a and 802.11g are 800 ns, allowing for path differences of approximately 240 meters. The default for 802.11n is also to use 800 ns, but if the multipath environment is not as strict about a required allowance for 240 meters difference in path between transmitter and receiver, 802.11n also provides a reduced guard interval of 400 ns. This reduces the symbol time from 4 microseconds to 3.6 microseconds and thus increases the data rate. For 20 MHz channels maximum data rates for one to four transmitters with the reduced guard interval are 72, 144, 216 and 288 Mbps and for a 40 MHz channel 150, 300, 450, and 600 Mbps.

3.2.4 MIMO channel estimation process

MIMO channel estimation is used for calibration and calculation of the transmitter steering matrix as well as the set of link parameters called Modulation Coding Scheme (MCS) that includes: optimum number of spatial streams, modulation format and data rate on each stream.

Measurement of the MIMO channel requires additional training periods to the ones used for 802.11a. Below is shown a PHY Protocol Data Unit (PPDU) for the HT mixed configuration, that has both HT and non-HT fields so that it can be

received by non-HT STAs. In the HT greenfield format, all of the non-HT fields are omitted.

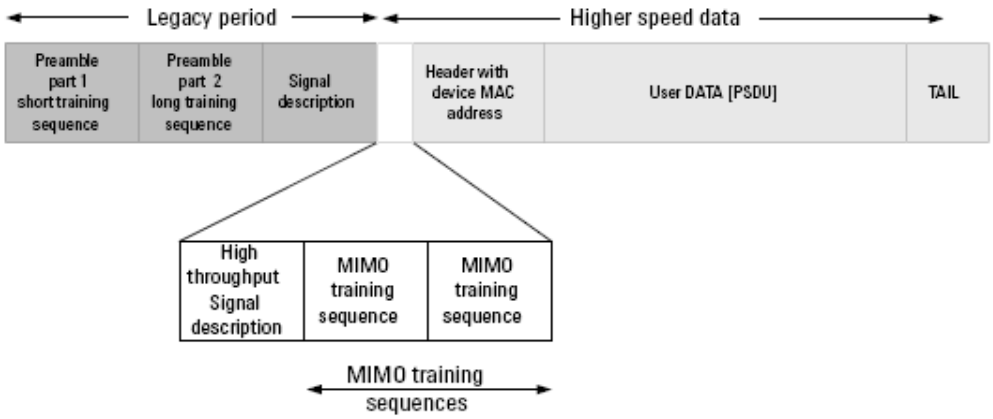

Figure 12: WLAN PHY protocol data unit in HT mixed format

The specific HT fields used are:

HT SIGNAL: Provides all the information required to interpret the HT packet format.

HT Short Training Field: For automatic gain control setting, timing acquisition, and coarse frequency acquisition.

HT Long Training Fields: Provided as a way for the receiver to estimate the channel between each spatial mapper input and receive chain, there can be one or several. The number of HT long training fields necessary to decode the HT-Data portion of the PPDU is determined by the number of space-time streams transmitted unless additional dimensions are optionally sounded using extension HT long training fields when it is desirable to obtain as full a characterization of the channel as is possible. These cases of MIMO channel measurement are referred to as MIMO channel sounding.

3.2.5 Link adaptation

To make the most out of the MIMO channel variations and transmit beamforming, both ends can dynamically negotiate and update the MCS. There are 77 MCSs that can be used either for 20 MHz or 40 MHz bandwidth in the current 802.11n draft, of which MCSs 0 to 15 at 20MHz are mandatory for an AP and 0 to 7 at 20MHz for a STA.

Link adaptation is optional and starts with MIMO channel sounding using the preamble training fields in a frame, then estimation of the MCS at the other end of the link and finally feedback to the transmitter.

The algorithms for implementation of rate adaptation are not covered in the standard and differ from vendor to vendor. Packet loss can occur during the adaptation procedure and that is why the speed of rate adaptation must be optimized in order to minimize loss of data. The rate adaptation affects throughput, delay and

jitter. Mobile devices are more exposed to power variations triggering the adaptation algorithm.

3.2.6 Transmitter beamforming

In order for the transmitter to perform beamforming it needs to calculate an appropriate steering matrix, task for which it needs the assessment of a receiver. The transmitter, initiator of transmission, is the beamformer and the receiver of the beamformed frame is the beamformee. The following two methods are specified in [6] 9.17 and 20.3.11 to estimate the coefficients in the steering matrix, a more didactic explanation can be found in [8]:

Implicit feedback: The beamformer requests a sounding frame from the beamformee and estimates the MIMO channel from the reception of the long training symbols in the frame, under the supposition that the channel can be considered reciprocal.

Calibration of the transmitter and receiver chains improves the performance of transmit beamforming using implicit feedback, because the differences between them degrade the inherent reciprocity of the over-the-air channel, and cause degradation of the performance of implicit beamforming. Over-the-air calibration is described in 9.17.2.4 [5].

Explicit feedback: The beamformee makes an estimation of the channel coefficients from training symbols sent by the beamformer, quantizes it and sends it to the beamformer. The beamformer can use the feedback to determine steering vectors.

3.2.7 Antenna selection

When the number of RF chains is smaller than the number of antenna elements at a STA or AP, antenna selection is a time-variant mapping of the signals at the RF chains onto a set of antenna elements. The mapping can be chosen based on instantaneous or averaged channel state information. Antenna selection requires the training of the full size channel associated with all antenna elements, which is obtained by transmitting or receiving sounding PPDUs over all antennas. When both transmitter and receiver have antenna selection capabilities, training of transmit and receive antennas can be done one after another. Antenna selection supports up to eight antennas and up to four RF chains.

3.2.8 Space-time block coding

Multiple input single output technique used to generate a more robust transmission path that allows achieving the same performance with two transmitting antennas as using maximum ratio combining with two receiving antennas as shown by Alamouti in[9].

In the name of the technique, the “space” refers to the separation of the antennas in the transmitting side and the “time” to the reversal of the transmission time of pairs of OFDM symbols. Each antenna is sending a different symbol from a different location at a time. Pairs of symbols have to be recovered and processed together in the receiver [2].

In the next figure, examination of the transmitted signals shows the additional phase rotations applied to each channel.

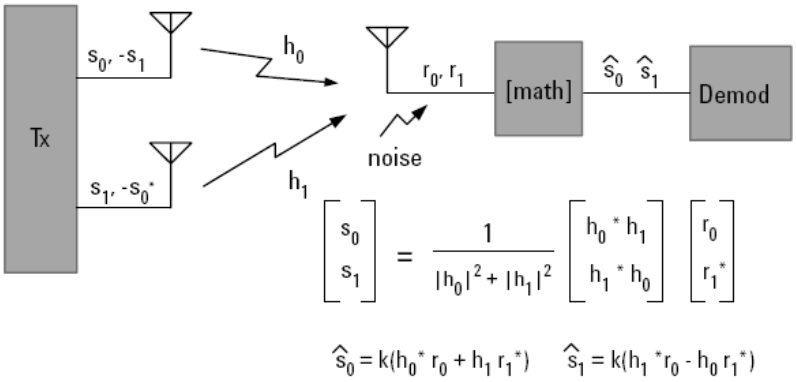

Figure 13: OFDM symbol manipulation used in space time block coding

3.3 WLAN HT MAC

The HT-MAC is based on the MAC layer of the basic 802.11 standard [1] and the Carrier Sense Multiple Access with Collision Avoidance (CSMA/CA) protocol. When a STA has performed association with an AP, the frame exchange can begin according to the following procedure. The STA senses the channel to determine if it is idle or not. If idle, before starting to actually send, the STA waits for a random period of time. If the channel is not idle, the STA chooses a random backoff value to start a counter and probes the channel at a certain rate, decreasing the counter value when the channel is sensed idle again, transmission will start only when the counter has reached zero.

The goal of multiplying the effective throughput of 802.11 standards cannot be achieved by only increasing the physical link rate. It is also needed to reduce the inherent overhead of the MAC protocol, the interframe spaces and acknowledgements of each frame transmitted. At the highest of data rates, the overhead alone can be longer than the entire data frame. In addition, contention to access the media and collisions also reduce the maximum effective throughput of 802.11. Below is an explanation of the main improvements 802.11n second draft proposes to the MAC layer. Further details can be found in [10] and [6].

3.3.1 Aggregation

All the frames transmitted have a fixed overhead consisting on a radio preamble and MAC frame fields that limit the effective throughput. See figure below:

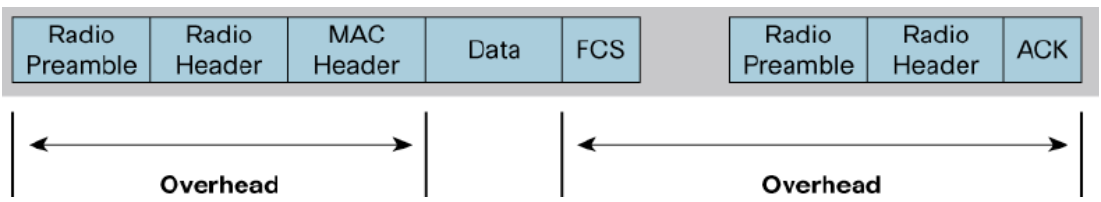

Figure 14: 802.11 MAC protocol overhead

The idea in 802.11n to reduce this overhead is frame aggregation. Frame aggregation consists basically on putting two or more frames together into a single transmission, as shown in the next figure:

Figure 15: 802.11n Frame aggregation

This reduces the number of potential collisions and the time lost to backoff. The maximum frame size is also increased in 802.11n from 4 KB to 64 KB for these larger aggregated frames.

A limitation of frame aggregation is that all the frames that are aggregated into a transmission must be sent to the same STA or AP. Another limitation is that all the frames to be aggregated have to be ready to be transmitted at the time, potentially delaying some frames to wait for additional frames in order to attempt to send a single aggregate frame. A third limitation of aggregation is the channel coherence time, the time over which the radio channel remains unchanged. Transmission time should not exceed the coherence time and so the maximum frame size that can be successfully sent is limited by this factor. Channel coherence time depends on the speed of transmitter, receiver and other items in the environment. The faster things are moving, the smaller the maximum frame size can be, with the implication that the data rate is reduced.

The 802.11n standard describes two methods for aggregation with differences in the efficiency gained. These can be better understood with the help of the following diagram:

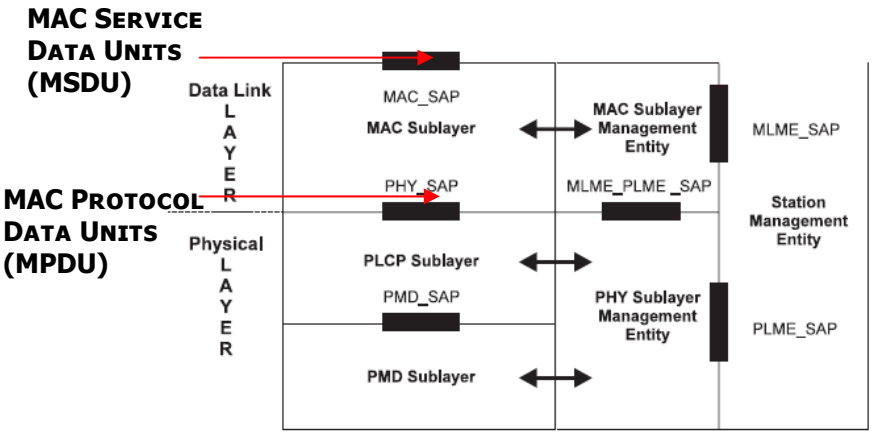

Figure 16: Architecture of the MAC and PHY layers with indications of where MSDUs and MPDUs are originated

MAC Service Data Units Aggregation: MSDU aggregation is the most efficient aggregation method. It relies on the fact that APs receive frames from its Ethernet interface to be translated to 802.11 frames and then transmitted to a STA, what means the native format of the frame is Ethernet. A number of Ethernet frames are compiled in a single 802.11 frame and then a single preamble and header added to

the aggregated MSDU. This method is more efficient than MPDU aggregation, because the Ethernet header is much shorter than the 802.11 header.

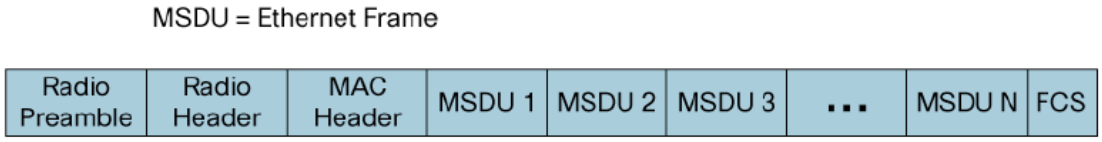

Figure 17: MAC Service Data Units Aggregation

MAC Protocol Data Units Aggregation: Instead of collecting Ethernet frames, MPDU aggregation translates each Ethernet frame to 802.11 format and then collects the frames for a common destination. The collection doesn't require a wrapping of another 802.11 frame, since the collected frames already begin with an 802.11 MAC header.

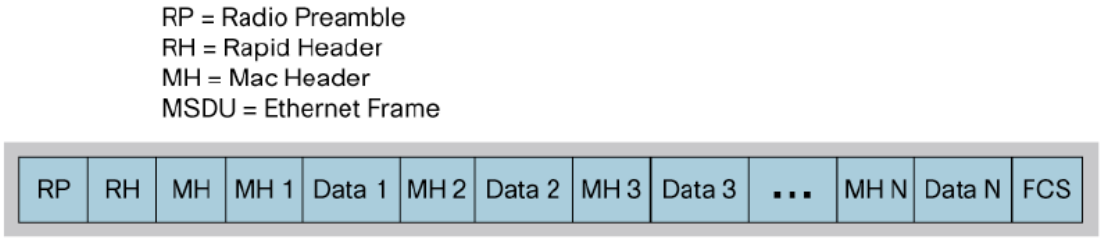

Figure 18: MAC Protocol Data Units Aggregation

3.3.2 Block Acknowledgement

For the 802.11 MAC protocol to operate reliably, each of the frames transmitted to an individual address (neither multicast nor broadcast frames) is immediately acknowledged by the recipient. MSDU aggregation requires no changes to this operation. The aggregated frame is acknowledged just as any 802.11 frame is acknowledged for MSDU aggregation. For MPDU aggregation, each of the individual constituent 802.11 frames must be acknowledged. To deal with this requirement, 802.11n introduces block acknowledgement.

Block acknowledgement compiles all the acknowledgements of the individual constituent frames produced by MPDU aggregation into a single frame. This allows a compact and fast mechanism to implement selective retransmission of only those constituent frames that are not acknowledged. In environments with high error rates, this selective retransmission mechanism can provide some improvement in the effective throughput of a WLAN using MPDU aggregation over that of one using MSDU aggregation, because much less is retransmitted when an error affects some of the constituent frames of an MPDU aggregated frame as compared to an MSDU aggregated frame.

3.3.3 Reduced Interframe Space

This mechanism reduces the overhead involved with transmitting a stream of frames to different destinations. It reduces the time between receiving a frame, typically an acknowledgement frame, and sending a subsequent frame. Reduced inter frame space cuts down the dead time between frames, increasing the amount of time

in the transmit opportunity that is occupied by sending frames. Reduced inter frame space is restricted to greenfield deployments, those where no legacy devices operate in the area.

Chapter 4: State of the art on measurements of WLAN devices

The dual nature of WLAN, as a radio communication standard and as a computer network protocol, has raised two main different approaches to its characterization: *RF Performance* and *Throughput Benchmarking*. Each of them offers information at a different Open Systems Interconnection (OSI) model layer.

4.1 RF performance

The CTIA and IEEE have established two different RF testing methodologies for WLAN devices. For information on the CTIA and the IEEE see Appendix I.

4.1.1 IEEE

The IEEE standard establishes a comprehensive set of RF specifications for 802.11n devices, comprised in [6] 20.3.20 and 20.3.21. These include *transmit spectrum mask, spectral flatness, transmit power, transmit centre frequency tolerance, packet alignment, symbol clock frequency tolerance, transmit centre frequency leakage, transmitter constellation error* and *transmitter modulation accuracy (EVM)* for the transmitter, and for the receiver: *minimum input sensitivity , adjacent channel rejection, non-adjacent channel rejection, receiver maximum input level* and *clear channel assessment sensitivity*. Here are also defined the measurement methodologies to follow, that mostly consist on cabled measurements referred to the antenna connector.

WLANs implemented in accordance with these, satisfy only minimum requirements for interoperability and are subject to operating requirements and equipment certification methods established by regional and national regulatory administrations.

Measurements of transmitted power and receiver sensitivity are defined as:

Maximum allowable transmit power must not go beyond the regional limit in any case and is independent of the number of antennas in the device. The Federal Communications Commission of the United States defines it as power at the antenna connector when the antenna gain is less than 6dBi [5].

Receiver sensitivity is defined in [6] as the minimum input level that results on a packet error rate (PER) of less than 10% for a PSDU length of 4096 octets. These minimum input levels are measured at the antenna connectors and referenced as average power per receive antenna. Each transmitting port at the WLAN simulator must be connected to a port of the DUT, and the number of spatial streams under test shall be equal to the number of utilized transmitting ports and also equal to the number of utilized DUT input ports. The minimum sensitivity level is specified in Table 1: Minimum receiver sensitivity, from [6].

Modulation	Rate (R)	Adjacent channel rejection (dB)	Non-adjacent channel rejection (dB)	Minimum sensitivity (dBm) (20 MHz channel spacing)	Minimum sensitivity (dBm) (40 MHz channel spacing)
BPSK	1/2	16	32	–82	–79
QPSK	1/2	13	29	–79	–76
QPSK	3/4	11	27	–77	–74
16-QAM	1/2	8	24	–74	–71
16-QAM	3/4	4	20	–70	–67
64-QAM	2/3	0	16	–66	–63
64-QAM	3/4	–1	15	–65	–62
64-QAM	5/6	–2	14	–64	–61

Table 1: Minimum receiver sensitivity in the 802.11n third draft of the standard

4.1.2 CTIA

CTIA test techniques for mobile phone standards currently on the market are well known and consist on combining traditional spherical antenna pattern measurement in anechoic chamber with the test equipment necessary to establish a voice or data connection to the phone in order to measure transmitted power and receiver sensitivity at each position of the pattern, see details in references [11] and [12].These are active measurements, in which the signals used to test the device are the ones in the communications standard to be used. They provide a realistic approach to the real overall device performance because interactions between the antenna, the body of the phone, the circuitry in the phone and the near-field environment are also taken into account. This results in performance characterization that differs significantly from that predicted by combining conducted radio performance (through a 50Ω cable) with measured performance of the antenna. Since the phone is operating with an active transmitter or receiver, the resulting pattern is in absolute power units (as opposed to a typical relative radiation pattern), so that integration of the surface produces device performance metrics such as total radiated power (TRP) and total isotropic sensitivity (TIS).

In response to the growing number of cellular devices starting to have WLAN capabilities and vice versa, the CTIA released in August 2006 and then updated in August 2007 its "Test Plan for RF Performance Evaluation of Wi-Fi Mobile Converged Devices" [13]. This document defines the test methodology for the RF Testing of both converged cellular-WLAN devices and WLAN APs in the 802.11a, b and g standards, and specifies conducted as well as radiated tests in anechoic chamber with the device placed in a standard operational mode. No support for 802.11n devices is defined and most of the RF parameters taken into account have not been defined for devices with MIMO yet. The performance metrics in this methodology are the following:

Total radiated power: TRP refers to the power leaving a closed surface which surrounds the AP or the converged phone when it is located far from other objects. It is the maximum available power that would be radiated by the phone if the antenna was ideally matched to the output impedance of the phone, minus the power reflected due to the actual mismatch at the antenna port, minus the power dissipated in the antenna, minus the power absorbed in the head phantom. In the CTIA measurement setup it is measured from the ACKs the DUT generates in response to a stream of 200 bytes long

frames composed of uniform data content at a rate of 50 frames a second, to approximate a voice data stream. It is the figure of merit of a device in transmit mode.

Total isotropic sensitivity: TIS refers to the minimum received power level at which the digital error rate of the AP or converged phone in receive mode reaches a specific limit. The CTIA definition of TIS is 10% frame error rate (FER) for 200 bytes test frames at a rate of 50 frames a second, to approximate a voice data stream. It is found by lowering the transmit power level of the WLAN base station simulator until the specified digital error limit is reached. The power required to obtain the error limit is the value of the sensitivity, that represents the figure of merit of the device in transmit mode.

Radiated WLAN Receiver Sensitivity Degradation on Simultaneous Operation: Degradation of the TIS of the converged device in WLAN mode when it is operating in cellular and WLAN modes at the same time. The testing procedure is the same as for the TIS with the addition of a cell phone base station emulator that establishes a call with the device in cellular mode transmitting at full power.

Radiated Cellular Receiver Sensitivity Degradation on Simultaneous Operation: Tests the degradation of the TIS of the converged device in cellular mode when it is operating in cellular and WLAN modes at the same time. The testing procedure is equal to the one in CTIA cellular test plan [11] except for the DUT answering on its WLAN interface to unicast packets sent by a WLAN AP at the same time. A reference measurement of the TIS of the device in cellular mode must be provided for comparison.

4.2 Throughput Benchmarking

The Internet Engineering Task Force (IETF, see more in Appendix I) understood at the start of the 90's the need for a uniform approach to benchmarking shared across the industry, and formed the Benchmarking Methodology Working Group to carry out this assignment. IETF requests for comments have an informative approach and are not considered as standards.

The first RFC was "Benchmarking Terminology for Network Interconnection Devices" [14], in 1991, giving definitions of a number of terms that are used in describing performance benchmarking tests and the results of such tests.

The definition of *throughput* given by that document is "the maximum transmission rate at which none of the offered frames are dropped by the device. Measurements should be taken over an assortment of frame sizes. If there is a checksum in the received frame, full checksum verification must be done". Note that here frames and rate refer to OSI level 2 figures. Since the loss of a single frame in a data stream can cause significant delays for the higher level protocols, it is useful to know the actual maximum data rate that the device can support and this is the main figure of merit that used in later performance benchmarking.

Since then, several generations of test tools have evolved, providing accurate and repeatable performance test results. However, these testing techniques meant for wired devices disregard the complexities of the WLAN physical layer and transmission protocols. The random nature of the propagation over the air and the exposure to

uncontrolled interference cause unpredictable fluctuations in the throughput, which in turn make highly challenging to acquire repeatable measurements. Until now throughput measurements have been carried out with the following methodologies:

4.2.1 Field tests

The first approach to WLAN testing have been *field tests* in which engineers deploy a network setup in a certain environment dedicated to the test, such as a house or an empty office building. Then they place the WLAN devices on mobile carts, moving to various locations in the test space, manually configuring tests and recording test results at each location. The presence of undesired interference is optionally checked with a spectrum analyzer and when interference appears, the test has to be discarded and restarted after waiting for the disturbance to be gone.

The effectiveness of these tests is strongly limited by the severe dependence on the location, the possibility of unnoticed interference and the time consuming manual test setup.

4.2.2 Measurements in shielded chambers

Throughput performance is also often tested in shielded environments to avoid the effect of interference [15]. While this is certainly an improvement over field tests, it may be not fully representative for the normal operating conditions of WLAN devices.

If the chamber walls are absorptive, then there exists only line of sight communication, whereas most of the WLAN operation takes place in non-line of sight multipath environments and 802.11n devices are explicitly designed for them.

The case of the chamber walls being reflective is the case of the reverberation chamber, but without stirring mechanisms implemented there is just a single realization of the multipath conditions that does not allow a representative statistical distribution that fully describes the average throughput in those conditions.

4.2.3 Isolated Cabled Test Beds

In isolated cabled test beds all devices under test are set in individual shielded enclosures are connected by cables to programmable RF attenuators, combiners and switches. This test methodology replicates the WLAN network in a controlled, cabled environment, removing any fading or interference. The two following figures belong to [16] and illustrate the difference between an isolated cabled test and an over the air test. The throughput of a WLAN system was measured both with the antennas removed and the devices set in a cabled test bed and with the antennas connected and the system exposed to the effects of propagation and interference.

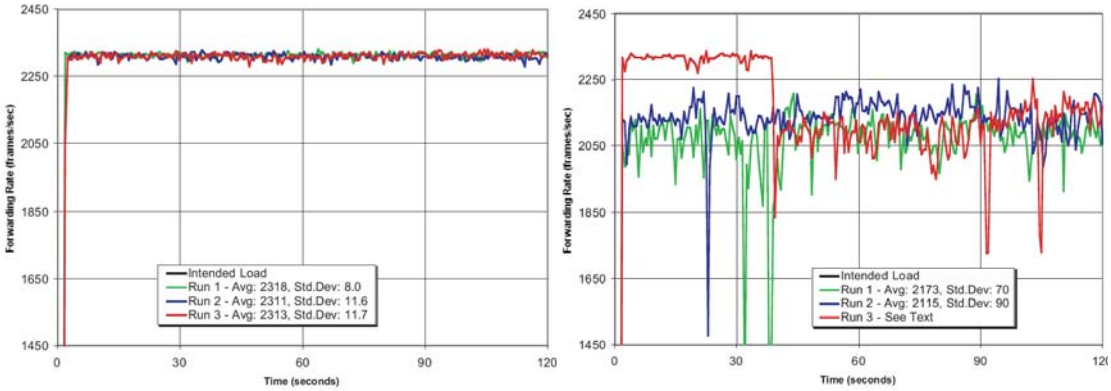

Figure 19: Three iterations of an 802.11a throughput measurement over two minutes in an isolated test bed to the left and under uncontrolled fading and interference to the right

The isolated cabled environment gives very good repeatability and little deviation compared to the over the air test. It serves well for verification of the transmitter and receiver, but does not provide a figure that illustrates their performance in normal working conditions, where fading and interference are undoubtedly present. Besides, this approach is not valid for devices with MIMO, which are specifically designed to work under fading conditions.

4.2.4 Channel emulators

In order to make test results more realistic and closer to the real user experience, a channel emulator can be added to the previous isolated test bed setup between the transmitter and receiver.

A channel emulator basically consists of a finite impulse response digital filter implemented in a digital signal processor, whose inputs correspond to the down-converted transmitter signals at the antenna connectors. The filter output is up-converted and fed at the receiver antenna connectors. The channel emulator provides this in both directions of communications to emulate properly the over the air transmission. Extensive information about channel emulation can be found in [17].

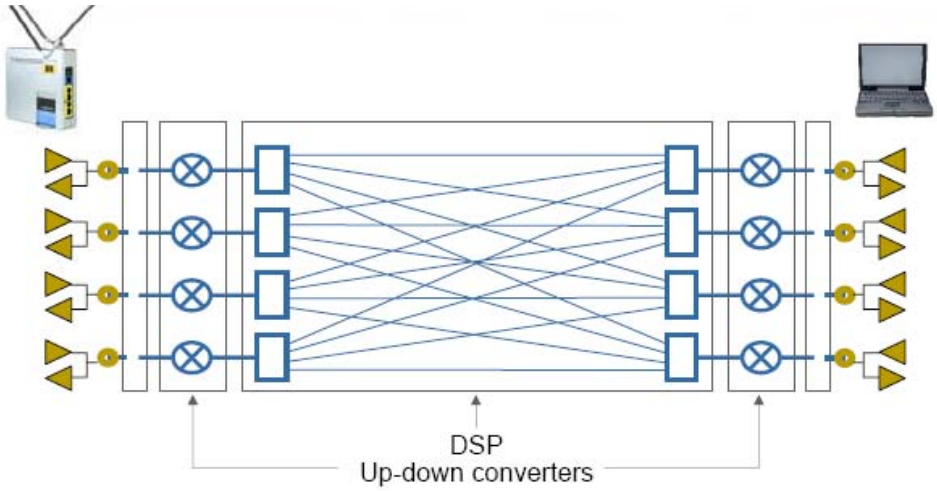

Figure 20: Diagram of a 4x4 channel emulator

A range of fading environments with different statistics can be implemented by adequately programming the filter coefficients according to stochastic process models. There are a number of channel models that are defined by standard organizations to create a baseline for comparison between devices of the same protocol. ITU M.1225 Pedestrian B and Vehicular A channel models are defined to test WiMAX devices and IEEE 802.11n channel models A through F are used for WLAN. The table below shows the parameters of IEEE 802.11n channel models A through F [18].

	Models					
Parameters	A	B	C	D	E	F
Avg 1st Wall Distance (m)	5	5	5	10	20	30
RMS Delay Spread (ns)	0	15	30	50	100	150
Maximum Delay (ns)	0	80	200	390	730	1050
Number of Taps	1	9	14	18	18	18
Number of Clusters	N/A	2	2	3	4	6
Rx and Tx Antenna Spacing	1/2,1, 4 λ					

Table 2: 802.11n TGn channel models

Below is shown a snapshot of the throughput measurement software implemented in a fading simulator. The measurement corresponds to the average throughput measured as a function of the channel model and the large scale path loss.

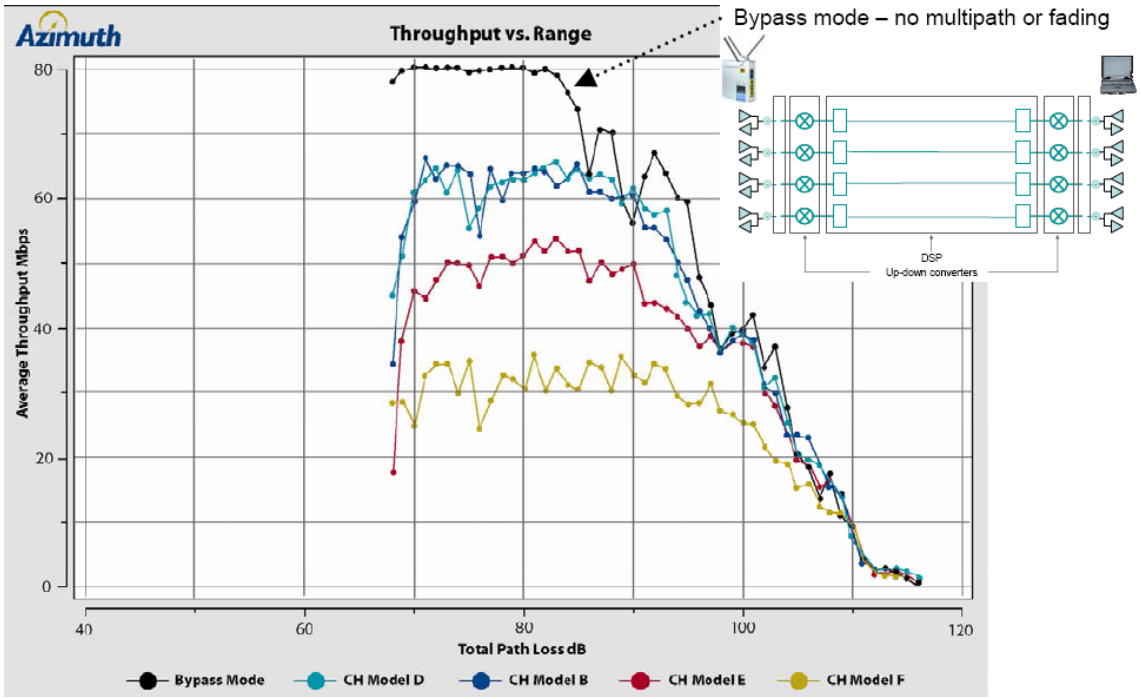

Table 3: Measurement of the average throughput of an 802.11n device as a function of the large scale path loss for different channel models in a fading simulator

Compared to the bypass mode that corresponds to the cabled test bed with no added fading, the throughput in multipath is at least 15Mbps lower and can be further reduced 35Mbps more if the environment is harsher for a fixed path loss of 80dB. This shows the need for characterization in multipath when assessing the user experience.

Despite the fact that channel simulators can provide a good benchmarking method for the radios, they offer a measurement that disregards the full complexity of the antenna system, since the models cannot precisely account for all the possible details of antenna configurations like polarization, correlation and efficiency that are known to impact diversity and MIMO channel capacity.

Chapter 5: RF Characterization of the AP

The device under test is a D-Link RangeBooster N 650 Wireless Router (model DIR-635) with operation restricted to the 2.4 GHz ISM band. It features Atheros XSPAN Technology AR5008 [19], which was the first series of chipsets based on the draft 802.11n specification. This is a series of two-chip solutions based on a triple-radio chip (model AR2133) paired with a baseband processor and media access controller chip (model AR5416). The triple-radio RF design of the router delivers up to 300 Mbps physical data rate at 40 MHz bandwidth operation and achieves, on average, 50 percent greater sustained throughput at range than 2x2 MIMO systems. Proprietary algorithms have been implemented to increase link robustness and throughput by simultaneously transmitting across three spatially-diverse signal paths, and incorporating information from three receivers simultaneously within the signal processing at the receiver. This improves substantially the robustness achieved by switching a smaller number of simultaneous transmitters between additional antennas.

For the system test, a client STA for the AP is needed. The chosen one has been a D-Link RangeBooster N USB Adapter (model DWA-142), which is a two-antenna 802.11n draft compliant WLAN client.

A characterization of the MIMO AP transmitter was performed using the *Agilent N4010A wireless connectivity test set* together with the *Agilent N4011A MIMO multi-port adapter*. The instrument was operated via Ethernet by a computer running the Virtual Front Panel software [20].

5.1 Description of the measurement instrument

The N4010A is a single channel one-box communications tester that provides high-performance demodulation capability allowing the most important SISO radio transmitter parameters to be tested. These include single channel Error Vector Magnitude (EVM), carrier leakage and spectral flatness, in addition to power and spectrum measurements.

The multiple transmitters and receivers in the MIMO DUT require several iterations of the SISO measurements to be performed, besides some specific tests for MIMO such as isolation between channels. The solution implemented to use the N4010 single-port one-box tester for this purpose is the N4011A MIMO multi-port adapter, consisting on a switch matrix as seen in the diagram below. For other MIMO testing solutions, check [21].

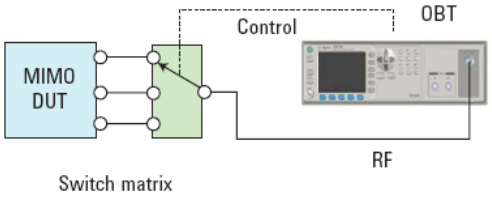

Figure 21: Block diagram of the switch matrix approach for MIMO testing

The MIMO transmitter measurement follows the multiple-captures-single-analysis approach. With the device connected to the instrument and transmitting continuously on all its ports, the measurement is triggered on the first frame in the first port of the capture order list. Then the switching matrix automatically changes the instrument input to the next port of the capture order list, re-arms the trigger, and captures a second frame. This goes on for as many ports there are in the capture order list.

The switching process is fast enough so that the frames can be rearranged as if they had been captured in parallel as shown in Figure 22.

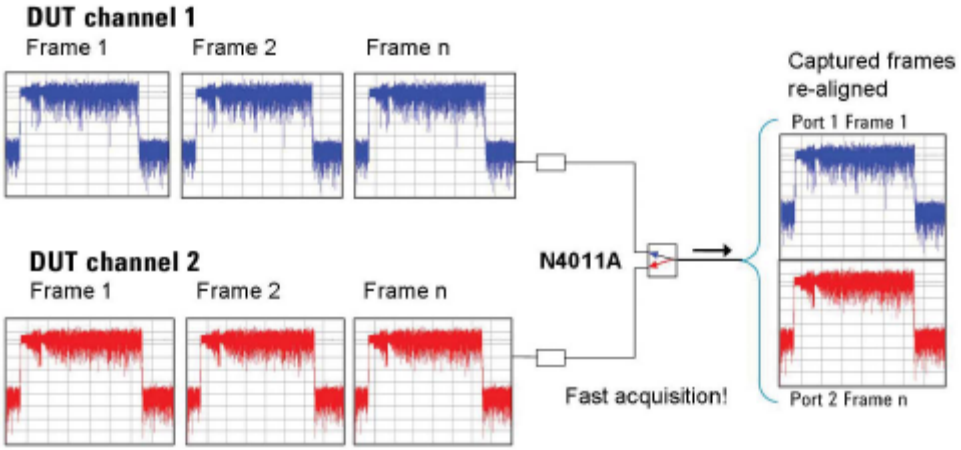

Figure 22: Sequential capture process of a two-channel MIMO signal

The data obtained in this way is passed to the demodulation algorithm, which solves the MIMO channel matrix and demodulates the channels as if acquired simultaneously, yielding a full range of demodulation results, including EVM per channel and per stream, burst power, cross power, channel response, and protocol burst information.

5.2 Definition of parameters in the transmitter test

5.2.1 Transmit power

Transmit power measurements using the Agilent N4010A with the switch matrix give values for the individual DUT channel powers as well as for the total output power of the device.

5.2.2 Transmit spectral mask test

Transmit spectral mask measurements must be performed channel by channel in the N4010. The spectral density of the transmitted signal shall fit within the corresponding spectral mask defined by the standard, 20.3.20.1 [6].

5.2.3 Transmit cross-power and channel isolation

In a directly mapped MIMO device, in which each channel bears a single spatial stream, the cross-power value is the undesired power from adjacent spatial streams leaking into a certain channel, and the more isolated the different channels are the better. In the case of a device operating in spatially-mapped mode, any channel

isolation or leakage effects are masked by the deliberate expansion of spatial streams across transmitter channels, see 3.2.1/I in this report to see the different possibilities of implementation for spatial mapping. In this situation, the cross power values will provide a measure of the degree of spatial expansion used. This is illustrated in the following figure, where snapshots of the channel response of both a direct-mapped and a spatially-mapped unit are shown.

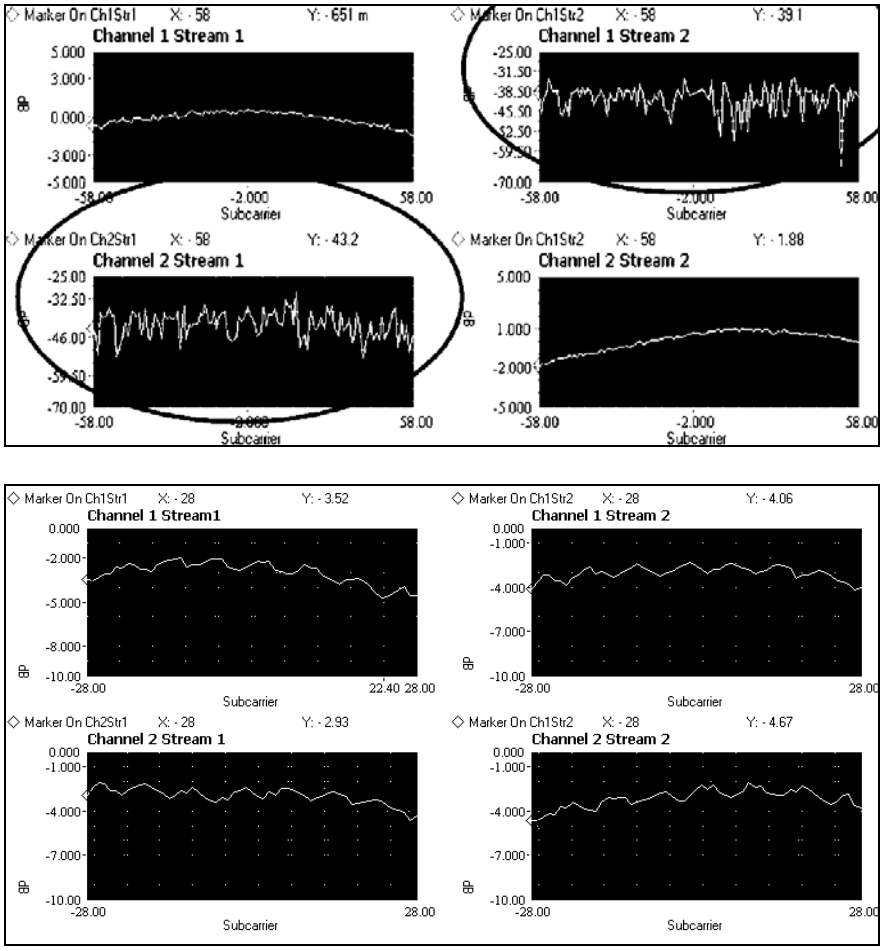

Figure 23: Comparison of the channel response of direct-mapped (above) and spatially-mapped devices (below)

The amount of power belonging to different spatial streams in a channel is similar in the figure below, whereas above there is a 40dB difference.

5.2.4 Transmitter Error Vector Magnitude

The EVM, also known as transmitter constellation error, is the root mean square of the error vectors at each detected symbol location. The error vector is the vector subtraction of the measured I/Q phasor minus the reference I/Q phasor (check the following phasor diagram).

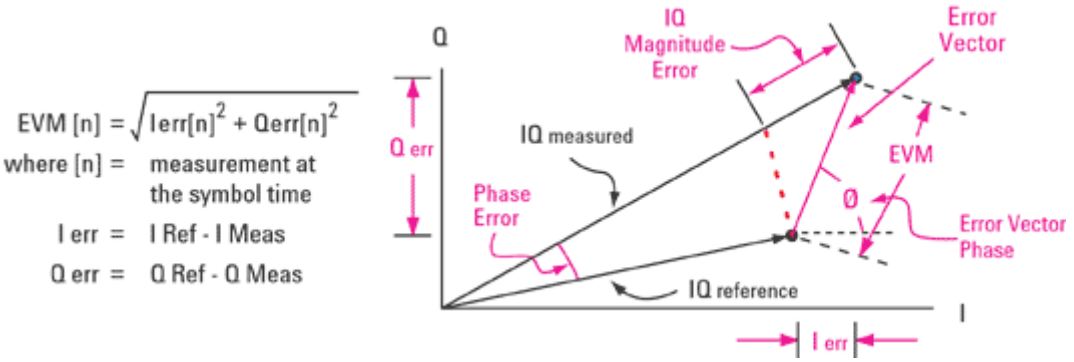

Figure 24: Definition of Error Vector Magnitude

In the 802.11 standards, it is expressed as a percentage of the square root of the mean power of the ideal signal, averaged over the number of symbols, spatial streams and frames measured. A detailed description of the measurement setup can be found in 802.11n 20.3.20.7.4 [6].

The EVM provides a measure of the modulation quality of a transmitter, both influenced by the digital operation of the MIMO radio as well as analog RF effects. Since the demodulation algorithm of the instrument used effectively solves the channel matrix, both spatial stream and channel EVM can be measured. When the DUT is in direct-mapped mode (each spatial stream is mapped directly to its corresponding transmitter channel), the channel and stream EVM values are the same. To be able to successfully demodulate spatially-mapped signals, the payload data and scrambler seed value remain constant from pulse to pulse.

The maximum EVM stated by the standard, averaged over subcarriers, OFDM frames and spatial streams, depends on the data rate and can be found in 20.3.20.7.3 [6]. The table has been reproduced here to provide illustration of the allowed EVM magnitudes.

Modulation	Coding rate	Relative constellation error (dB)
BPSK	1/2	–5
QPSK	1/2	–10
QPSK	3/4	–13
16-QAM	1/2	–16
16-QAM	3/4	–19
64-QAM	2/3	–22
64-QAM	3/4	–25
64-QAM	5/6	–28

Figure 25: Maximum EVM values in the 802.11n draft standard

5.3 Measurement setup

Unlike mobile telephony standards, WLAN devices do not implement a test mode. A special firmware is needed for this purpose and must be provided by the manufacturer and installed in the DUT. This firmware should allow continuous generation of dummy frames at different rates, disable of beacon signal and legacy

coexistence mechanisms, control of output power, switching on and off radio chains and control of spatial mapping of the device.

Some WLAN test sets implement the control of the DUT via the own WLAN signalling protocols and thus do not need such a special software, like Anritsu MT8860B, but this is not the case of the test instrument used.

The Agilent N4010 needs a continuous stream of frames at its input RF port to perform the measurement. Moreover, when the DUT performs spatial expansion, it is required that the payload data and scrambler seed value remain constant from pulse to pulse so that demodulation algorithm in the instrument works properly. As explained before, the optimal solution to generate this signal is to have a specific test firmware installed in the router. However, since this firmware is not commercially available, an alternative setup needed to be arranged so that the router would constantly send frames in the downlink. The solution found was to split the output signal at the antenna ports of the transmitter with directional couplers to allow connection with a STA via the original dipole antennas. This connection was filled with dummy frames of constant content by running the network traffic generator Iperf. However, no control over the scrambler seed value can be achieved and so the demodulation results will not be representative.

There was not laboratory equipment available to have three identically split branches and so it was decided that, since there are only modulation formats with two spatial streams in the router, it was possible to try to control their mapping of the signals in the antennas by terminating one of the antenna ports and connecting the other two. As will be shown later, this proved to be an erroneous approach since the device implements spatial mapping, although thanks to it some things about the DUT were learnt. The following figure shows a diagram of the measurement setup.

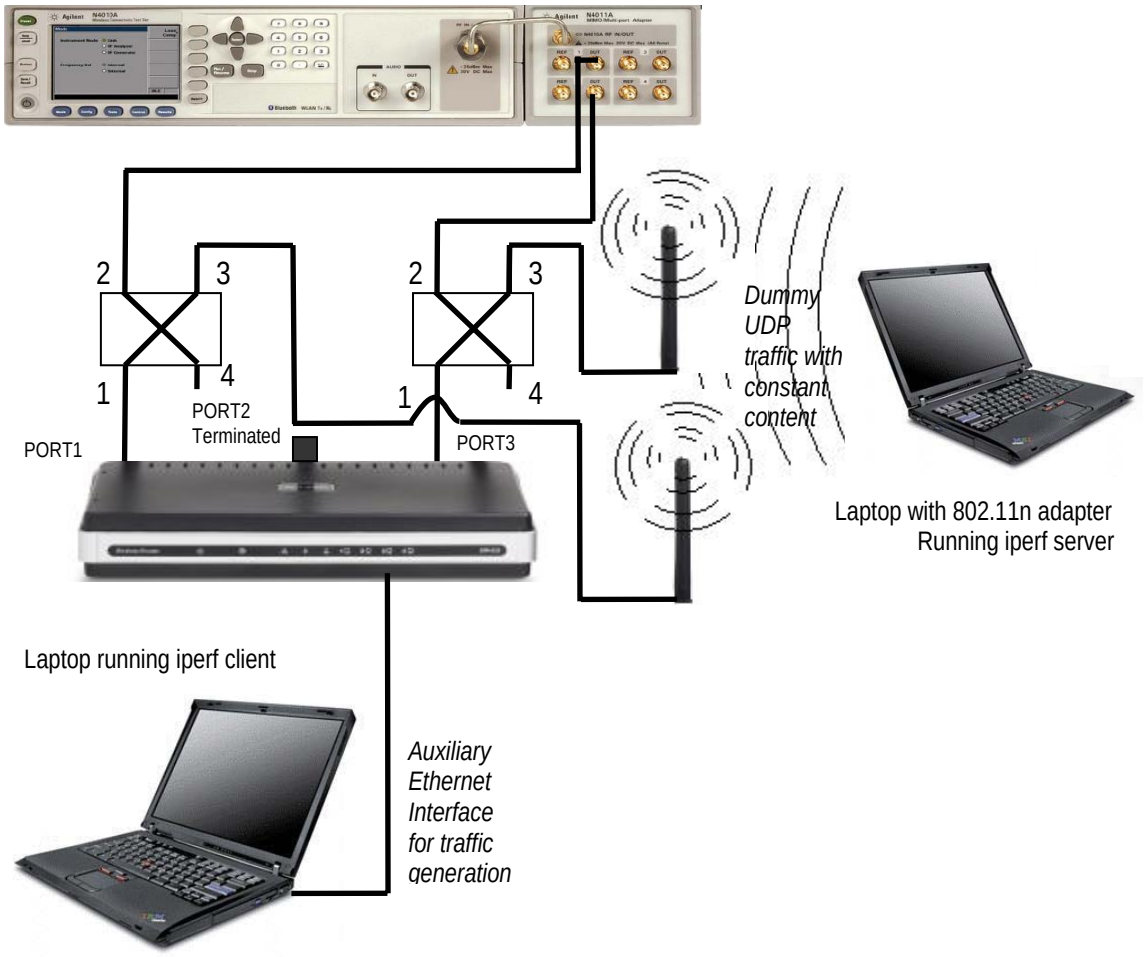

Figure 26: N4010 Measurement setup

5.4 Results

As mentioned before, the absence of specific testing behaviour in the router implies that the device is not only forwarding frames on its WLAN interface, but also doing other tasks implemented to manage connections and over which there is no control. This means that frames of other legacy protocols with modulation formats other than specified can appear and so a criterion to accept the measurements over the right frames of the modulation that is being evaluated must be set.

A validation of the measurement setup was performed with the Agilent Graphical Interface 89601A, that was connected to the own N4010A USB interface and run in parallel to the measurement in the Virtual Front Panel. This software provides spectrum, time-domain and modulation analysis for burst signals paired with graphical representation that enabled quick troubleshooting. This way it was possible to figure out the behaviour of the device and to establish that the measurement should be repeated until the following set of criteria was fulfilled:

- The signal must be correctly recognized as a *burst signal* by the instrument. This can be checked in the BurstGood field of the 802.11demod tab of the Virtual Front Panel.

- The *HT-SIG* status must be shown as correct and all the fields in the frame must be demodulated correctly.

- The *MCS* decoded from the header field must be the same as the MCS set in the DUT.

- The *modulation format* must be coincident with the one in the corresponding MCS.

- Since the frames are originally generated at a wired Ethernet interface, they keep their size when transmitted over the air. These frames will have a size correspondent to the Ethernet maximum transfer unit (1500 bytes) and the *Packet Length* property of the Virtual Front Panel will have a value of 1536 bytes due to the protocol overhead carried by the packet.

- *Overloading* of the measurement instrument must be avoided by setting an appropriate value in the PowerRange property of the Virtual Front Panel. Performing an auto range measurement can lead to a wrong numbers since it is not possible to control the kind of frames over which the auto range is made.

5.4.1 Frame format and MCS implementation in the DUT

By inspection of the Virtual Front Panel Burst Info tab, it was found that even if "only n" greenfield configuration is chosen in the router, the frames produced still keep the legacy training and signal fields of the mixed configuration, which is not compliant with the draft of the standard, check the frame format in 3.2.4, and slows down the transmission.

It was also discovered that while it is possible to choose any MCS number from 0 to 15 in the router, not all of them are implemented. MCS for two spatial streams with simple modulation formats that do not represent an increase of transmission rate (numbers 8, 9, 10, 11) are replaced by the MCS with highest rate in the single stream set (number 7). When link adaptation is enabled, this implementation leads to automatically switching to a modulation with a single spatial stream when the SNR is not high enough to drive a complex modulation. Thus, the advantage of spatial multiplexing is not taken when the SNR is low.

This was found by looking at the MCS number decoded from the frame header in Modulation Accuracy tab of the Virtual Front Panel and comparing it with the MCS set in the router. The results are shown in Figure 27.

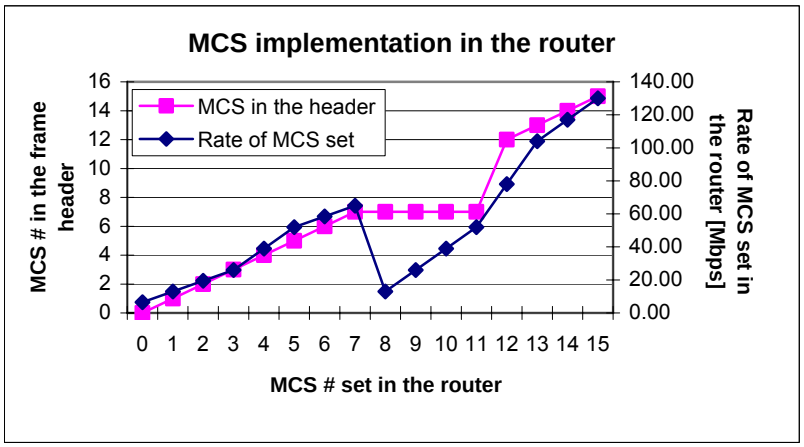

Figure 27: Implementation of the MCS in the router

5.4.2 Spatial mapping implementation

The channel frequency response resulting from demodulation of the spatial streams can show the kind of spatial mapping implemented on the device. In this case, and as shown in the snapshot from the Virtual Front Panel below, the device is configured in spatial expansion mode since the power levels for both streams are similar in both channels. Refer to the explanation of transmit cross-power and channel isolation in 5.2.3.

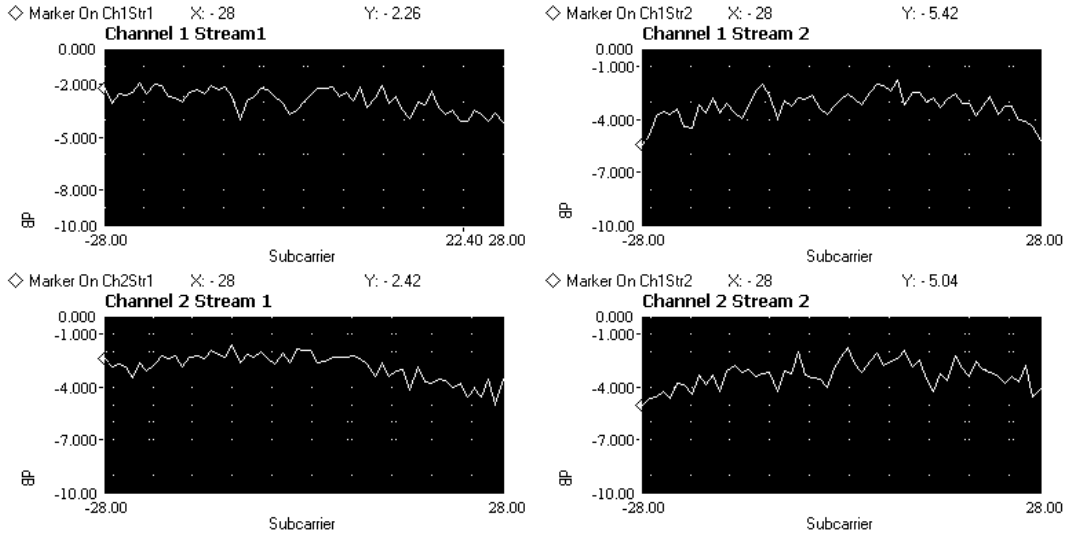

Figure 28: Router frequency response per channel and spatial stream

If the DUT implemented direct mapping plus antenna selection, then it would be possible to use the test setup suggested. However, since it is spatially-mapped it could be using the three antennas for transmission and that would invalidate the total transmitted power measurement as well as the EVM results, since with this setup one of the antennas is disconnected and terminated. Nevertheless, with the N4010 proper demodulation results are not achievable without a total control over the frame payload and the scrambler seed when the device performs spatial expansion.

The conclusion that can be drawn here is that WLAN RF testing needs specific a specific behaviour of the DUT for proper demodulation results and connection of all the antenna ports to the measurement instrument when the device is spatially mapped.

Chapter 6: Reverberation Chamber

6.1 Introduction

A reverberation chamber, also known as mode stirred chamber, consists on a metal cavity sufficiently large to support many resonant modes, which are perturbed with movable stirrers inside the chamber, creating a fading environment. A common usage of reverberation chamber is electromagnetic compatibility determination [22], but during the last years it has become increasingly popular for characterizing small antennas and wireless terminals in multipath environment.

Figure 29: Bluetest High Precision Chamber

Developed measurement capabilities in reverberation chamber include radiation efficiency of small antennas, TRP and TIS of active terminals with an accuracy similar to and often better than the one achieved in anechoic chamber. In the study in [23] the standard deviation between the results in the two chambers was 0.55 dB at 1800 MHz and 0.72 dB at 900 MHz.

Besides, measurements in the reverberation chamber are fast and easy to make in comparison with anechoic chambers and repeatable even in other reverberation chambers of equal or larger size, provided the chambers have efficient stirring methods. Another advantage is that reverberation chambers can be made of relatively small dimensions and still perform with high accuracy.

The fading environment in the chamber enables as well to measure diversity gain and maximum available capacity of MIMO antenna systems. An overview of several of the setups and references to other can be found in [24].

6.2 Description of the fading in the chamber

The number of independent plane waves at the receiver in the reverberation chamber is large enough so that the in-phase and quadrature components of the received signal are normally distributed, what results in a Rayleigh distribution of the magnitude and a uniform distribution over 2π of the phase. The power in the line of sight component is under normal circumstances much lower than the scattered power in the reverberation chamber, and can then be neglected. However, this depends on the Q-value of the chamber, which is conditioned by the chamber loading and size.

It has been shown that the reverberation chamber represents an isotropic multipath environment, in which the incoming waves have a uniform distribution in elevation and azimuth and all directions of incidence are equally probable, similar to that found in urban and indoor environments [25]. Moreover, different chamber sizes, stirring speeds and loading configurations allow flexible tuning of channel conditions in terms of delay spread [26] and Doppler shift [27] that can accommodate different propagation models.

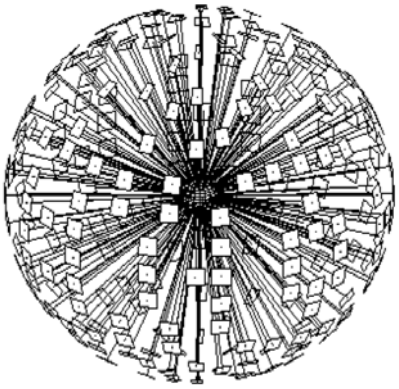

Figure 30: Distribution of angles of incidence in the reverberation chamber in 0.8m x 1.1m x 1m chamber (GSM 900 band)

Also as a result of the uniform distribution of the incoming waves, performance in the chamber becomes almost independent of the position of the antenna and any measurement becomes easier to set up.

6.3 Calibration of the environment in the chamber

Whenever the loading of the chamber varies, the environment characteristics change and so a reference measurement needs to be made. In the improved setup defined in 7.2.3 there are two laptops, a router, two stands, a USB adaptor and a head phantom present inside the chamber. The head phantom was included in the setup to increase the coherence bandwidth and provide a flat-fading that would not disturb the communication. This resulted on a quite heavy loading, providing a very large coherence bandwidth, as calculated below.

A reference measurement was performed in the 2.4 to 2.5 GHz frequency band using two 2.4 GHz dipoles of return loss smaller than 25 dB over this range. The dipoles were situated in the same positions of the router and the USB adapter during the measurement with the rest of the elements of the measurement setup inside the chamber. The addition of the loss due to the dipoles to the loading of the chamber during the reference measurement yields a measured coherence bandwidth slightly larger than the

existing one during the throughput measurement, but since there are much higher losses from other elements inside the chamber, this inaccuracy is expected to be moderate. Ideally the dipoles should have been present inside the chamber during the throughput measurement too.

The values of the S parameters were recorded over 180 seconds of continuous stirring sequence with a sample delay of 200 ms. The resolution of the network analyzer was set to 101 points. Two repetitions of the reference measurement were done, one with horizontal polarization and the other one with vertical polarization.

6.3.1 Coherence bandwidth

The transmissivity $S_{21}(f)$ is proportional to the complex frequency response of the channel $H(f)$ [28], and therefore calculation of the coherence bandwidth can be done in post-processing by finding the frequency separation Δf for which the frequency autocorrelation coefficient $\rho_{f,H,H}(\Delta f)$ falls below 0.5 at each stirrer position and averaging over all the positions of the sequence.

The frequency autocorrelation coefficient was defined in [29] as:

$$\rho_{f,H,H}(\Delta f) = \frac{\int_{-\infty}^{+\infty} H(\Delta f)\cdot H^{*}(f-\Delta f)\cdot df}{\int_{-\infty}^{+\infty} \left|H(\Delta f)\right|^{2}\cdot df}$$

Equation 4: Definition of frequency autocorrelation coefficient

Using this approach, the values obtained were B_C=9.5 MHz for the horizontal polarization and B_C=11.4 MHz for the vertical polarization, that result in delay spreads of σ_τ=21.05 ns and σ_τ=17.54 ns. The accuracy of this measurement could have been improved if it would have been performed over a larger frequency band centred in 2.45GHz.

Since the modulation format of the WLAN signal is OFDM, the symbol time is large enough to support large delay spreads. With a symbol time of T_{SYM}=4μs or T_{SYM}=3.6μs if the guard interval is reduced, it is assured that the symbol time is larger than the delay spread of the channel and thus the fading experienced by each of the carriers in the OFDM system is *flat*. It is not relevant that the fading over the whole system bandwidth is frequency selective because all the carriers are orthogonal and modulated at a slow symbol rate on a much smaller bandwidth.

6.3.2 Coherence time

Continuous stirring in a reverberation chamber causes Doppler shift larger than the one corresponding to the actual stirrer speed [27]. This behaviour is due to the resonances in the chamber, that enhance the effect of stirrer movement and dependent on the chamber Q-value.

The value of the Doppler shift that would cause fast fading is calculated from the maximum symbol duration, when the guard interval is not reduced. If T_{SYM}=4μs, to maintain the symbol duration well below the coherence time of the channel, it is set that $T_C > 10T_{SYM}$, then for $T_C = 10T_{SYM}$=40μs the maximum Doppler shift before the system

started to face distortion would be $f_D = \frac{0.423}{T_C} = 10.58 KHz$. This is a very high value that is not likely to be achieved in the usual applications of WLAN and that does not need to be reproduced in the chamber.

In spite of that, the most important effect of the Doppler shift is the increase of the bit error rate (BER) that exists even for slow fading channels and happens together with the appearance of a so-called BER-floor, a value of the BER that cannot be decreased by increasing the SNR. These effects depend on the channel coding and modulation format, so in 802.11n systems, different MCS will suffer a different impact.

In a system simulation, the speed generating a significant BER floor can be found and then assimilated to the equivalent stirring speed of the chamber.

Chapter 7: Throughput test in the reverberation chamber

Performance evaluation of throughput in WLAN MIMO devices is a challenging topic and currently there is not a testing method that covers the full system including the antennas, provides isolation from interference and reproduces realistic controllable radio propagation characteristics. As mentioned in 4.2, actual network installations show lack of repeatability due to uncontrollable interference and propagation complexities, measurements in anechoic chambers cannot reproduce the multipath environment in which MIMO devices are designed to perform and cabled test bed solutions that include multipath channel emulation do not assess the impact of the antennas in the system performance.

There is a demand in the industry for a full system RF test that complies with these needs. The measurement technique introduced in this report relies on the use of a reverberation chamber and a network traffic generator to provide transmission in a rich fading environment like the normal operation medium of WLAN devices. Measuring the effective link throughput at the transport layer payload, it makes possible to quantify the improvement in the quality of the user experience offered by different implementations of MIMO systems and WLAN standards.

7.1 Background

Several factors impact the performance of WLANs regarding throughput. These include:

7.1.1 Transport layer protocol and parameters

In computer networking, the transport protocol is the set of rules to transmit application data between two non-adjacent nodes transparently from the underlying network implementation. The most common transport protocols on the Internet are TCP (Transmission Control Protocol) and UDP (User Datagram Protocol). They have very different characteristics that may suit better one application or the other. TCP is used to deliver reliable communication, such as HTTP web browsing and email transfer. UDP typically gives higher throughput and shorter latency, and therefore it is often used for real time multimedia communication where occasional packet loss can be accepted, like in VoIP, IP-TV and online computer games.

UDP is the simplest of both protocols and does neither provide virtual circuits, nor reliable communication. The main parameter to be set is the requested bandwidth of the connection, that will be the offered traffic rate produced by the computer to load the link. Then there also are the send and receive buffer sizes, that amount to the space in the operating system kernel reserved to the communications protocol and fix the number of bytes sent or received at once. Since this is not a reliable protocol, packet loss will appear due to fading and must be accounted for.

TCP is more complicated, provides connection-oriented reliable communication over the underlying packet oriented datagram network, which involves

connection establishment, division of the data stream into packets called segments, segment numbering, reordering of out-of order data, error recovery by means of error detecting code, automatic repeat request, frame acknowledgement, flow control and congestion avoidance. This means more parameters to tune and to control in the measurement, as well as more delays induced by packet loss and retransmissions that could influence the repeatability of the measurement. The most important parameter that has an impact in TCP throughput is window size, which states the amount of bytes that can be transferred while there is no acknowledgement from the other side. Detailed explanations of the transport protocols can be found in [30].

Specific software for traffic generation needs to be used in order to control transport layer protocol and parameters. Two different programs have been used for this purpose and a brief explanation of their features can be found in the description of the measurement setup, section 7.2.

7.1.2 Wireless security algorithms

The extra computational effort added by security algorithms normally used such as WEP and WPA introduces delays and lowers the throughput, so it has been disabled because encryption is not in the scope of this study.

7.1.3 Quality of service

Neither differentiation of traffic classes and nor priorities have been established in these tests.

7.1.4 MAC frame size

In the uplink the fragmentation threshold is set to the default value of 2346 bytes and that is the maximum size of any frame to be transmitted. For the downlink, the control laptop generates the data flows and forwards them to the AP via its Ethernet interface, see the scheme of the basic measurement setup in Figure 31: Scheme of the basic measurement setup. As a result of this, the frame size is the Ethernet maximum transfer unit, which is 1500 bytes.

7.1.5 PHY configurations

The bandwidth for the transmission will be set to 20 MHz and the modulation coding scheme will be set as adaptive for all the measurements, unless otherwise stated, in order to allow connection in all the antenna configurations. If not, when the SNR is too low to establish a connection in a complex modulation format there is no throughput at all.

7.1.6 Channel characteristics

These are set by the stirring of the modes and the loading of the chamber. When the stirring is performed in a stepped sequence, the environment remains static during the whole measurement time whereas continuous stirring means a time-varying channel the system has to adapt to periodically.

The loading of the chamber allows modifying the losses and the delay spread of the channel. More considerations about the fading environment in the chamber can be found in 6.3.

7.1.7 Distance

The distance in a wireless system fixes the large scale attenuation and thus the power available at the receiver. In the context of WLAN, especially since it implements rate adaptation, this factor is critical for the performance in throughput. The present study does not cover variations of throughput derived of distance. The distance was fixed between 0.8 and 1.4 meters by the dimensions of the chamber and the stirring of the platform (see the setup in figure 33) and no extra attenuation than the one introduced by the chamber environment was accounted for. However, to reduce the high power values in the chamber, the output power of the router was set to low.

7.1.8 Interference

Interference is an important impairment to the throughput of WLAN devices mainly because of the implementation of the CSMA/CA (see 3.3) as the media access control protocol, that makes interference not only result in deteriorated receiver performance and increase of the bit error rate, but also in transmitter contention. The case in which the interfering signal is constantly present can result in impossibility to even start the communication.

WLANs operate in the unlicensed bands, where there are a large number of applications without the requirement for individual user or device licensing. Either co-channel or adjacent-channel interference from other WLANs, Bluetooth devices, cordless phones, wireless video surveillance cameras, wireless security and energy management systems, and computer peripherals like cordless mice, keyboards, and microwave ovens [31] can disrupt the WLAN transfer and reduce the link throughput.

Thus, it is of vital importance that the measurement setup is properly isolated and the chamber 100dB shielding maintained whatever connections have to be made.

7.2 Throughput measurement setup

In this study two different setups have been tried in order to evaluate the capabilities and necessities of this testing approach.

7.2.1 Basic setup

This has been the setup the study started with and that was later replaced by the improved setup.

Test layout in the chamber: The reverberation chamber used for both setups was a Bluetest High Performance model with an inner size of approximately 1.8 m x 1.75 m x 1.2 m, described in [32]. The basic test setup for the throughput measurement in the reverberation chamber is shown in Figure 31: Scheme of the basic measurement set and Figure 32: Pictures of the basic measurement setup. Both the router and the access point are placed inside the chamber with the latter over the turn table. A head phantom is used to load the chamber in order to increase the coherence bandwidth as discussed in [33].

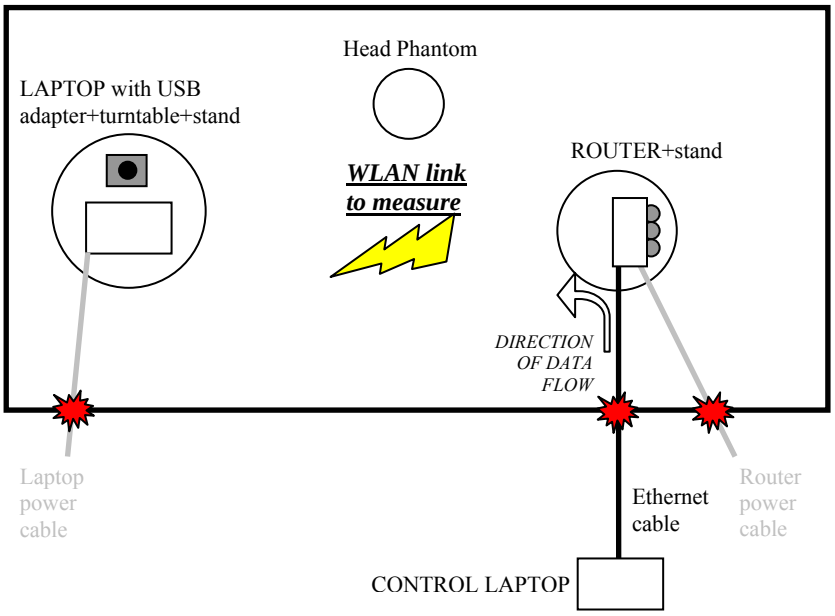

Figure 31: Scheme of the basic measurement setup

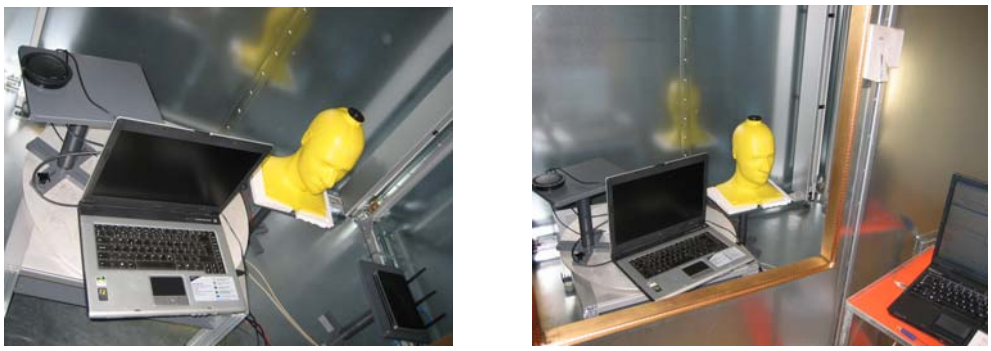

Figure 32: Pictures of the basic measurement setup

As stressed in Figure 31, there are three wired connections through the wall of the chamber: two of them are power cables to plug the router and the laptop inside the chamber, and then there is a third Ethernet cable to the control laptop where the data flow is originated.

Traffic generator software: Iperf, open source software developed by the National Laboratory for Applied Network Research of the United States [34] that can create TCP and UDP data streams and measure network throughput allowing modification of various parameters for network testing. In this setup the magnitude measured is the maximum unidirectional point-to-point link payload throughput between the computers.

Tests with Iperf were performed in TCP protocol because even though it implements UDP measurements, it is not possible to program the timeout to consider a packet lost and this biases the measurements of effective throughput in fading. The Nagle algorithm was disabled and the window size set to 128 KB to avoid unnecessary delays and get the highest throughput possible.

Iperf has client-server architecture and generates traffic from the client to the server. It was run on both laptops with the server in the laptop inside the chamber and the client in the control laptop, so that the flow of data was in the downlink direction (from the AP to the STA).

Test characteristics: The router operated always in the 2.4 GHz band with 20 MHz bandwidth and in 802.11n greenfield configuration with short guard interval, except for the measurement in the legacy configuration for 802.11g. Measurement times and number of samples of continuous and stepped sequences differ.

Continuous sequence: The measurement is performed over a 90 seconds continuous stirring sequence with sampling frequency of 2 samples/second. This was found to be long enough for a 95% confidence interval for the sample average smaller than 2 Mbps.

Stepped sequence: The number of different positions in the chamber is 50 and then a 10 second record with sampling frequency of 2 samples/second is made at each of the stirrer positions and averaged.

As shown by the first tests in section 7.3.1, the throughput is not affected by the continuous movement of the stirrers because of the robustness of the OFDM modulation and so results of continuous and stepped sequences have large correlation, with the advantage of the continuous stirring offering a shorter measurement time.

7.2.2 Problems and modifications of the basic setup

The main problem in the basic setup is the power leakage due to the cables that go through the wall of the chamber. This leakage makes it possible to connect to the AP even when the chamber is closed, which is a situation that must be avoided.

The fact that power is being conducted out of the chamber means that, in the same way, power can be conducted inside the chamber and cause interference. In fact, a rather unpredictable behaviour was detected in the channels of the lower part of the band and channel 2 shows lower values for the throughput than the other channels in the measurements taken in the basic setup but not in those in the advanced setup.

To solve this situation, the first measure was to filter the power getting to the chamber to feed the router and the laptop using the N-connectors at the walls as seen below.

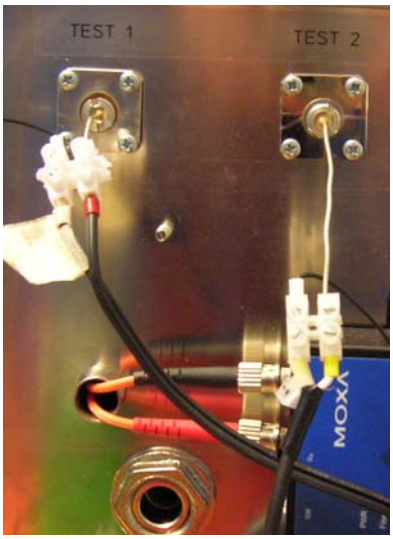

Figure 33: Power filters in the N-connectors

Then the power leakage remained through the Ethernet cable, and this could not be filtered because the transmission rate of the signals in it is quite large. The first measure tried was to establish an optic fiber link through the chamber wall with two Ethernet-to-fiber converters. This option was very effective removing the power leakage, nevertheless, it lowered the link throughput and so the idea was discarded.

The alternative chosen was to set the control laptop inside the chamber so that the whole length of the Ethernet cable remained inside and there was no leakage. Then the stirrers' movement had to be controlled from inside the chamber as well and synchronized with the program for the throughput measurement. This was implemented by a C++ program that united the calls to the Bluetest stirring-functions library with system calls to the execution of the measurement program, working for both Iperf and IxChariot, and the very simple graphical interface in Figure 34.

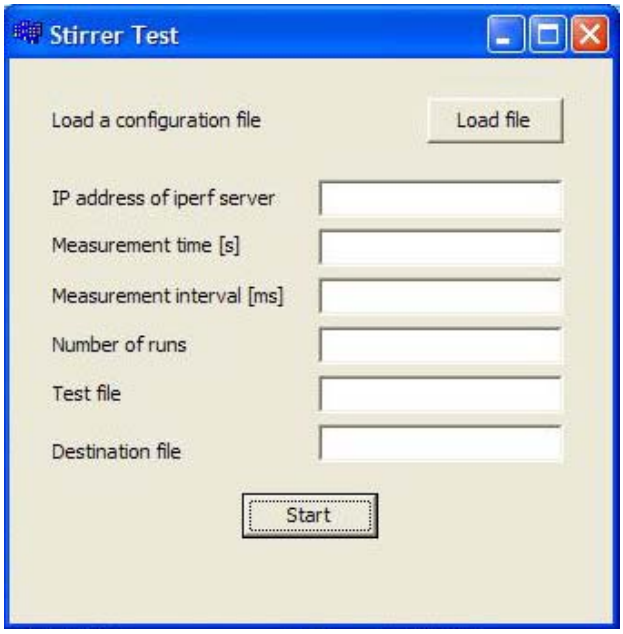

Figure 34: Improved setup software graphical interface

As a result of the control laptop being set inside the chamber, the connection to the serial interface that controls the motors for the mode stirring outside the chamber was not reachable, and another modification was performed. This consisted in directly connecting the control laptop to the stirrer controller card, which lies in a metal box inside the chamber, via a serial bus.

7.2.3 Improved setup

Test layout in the chamber: The chamber is still the Bluetest HP chamber, with the addition of the modifications mentioned and a cabled control interface in parallel to the wireless link so that control traffic does not influence the throughput measurement. A diagram is shown below.

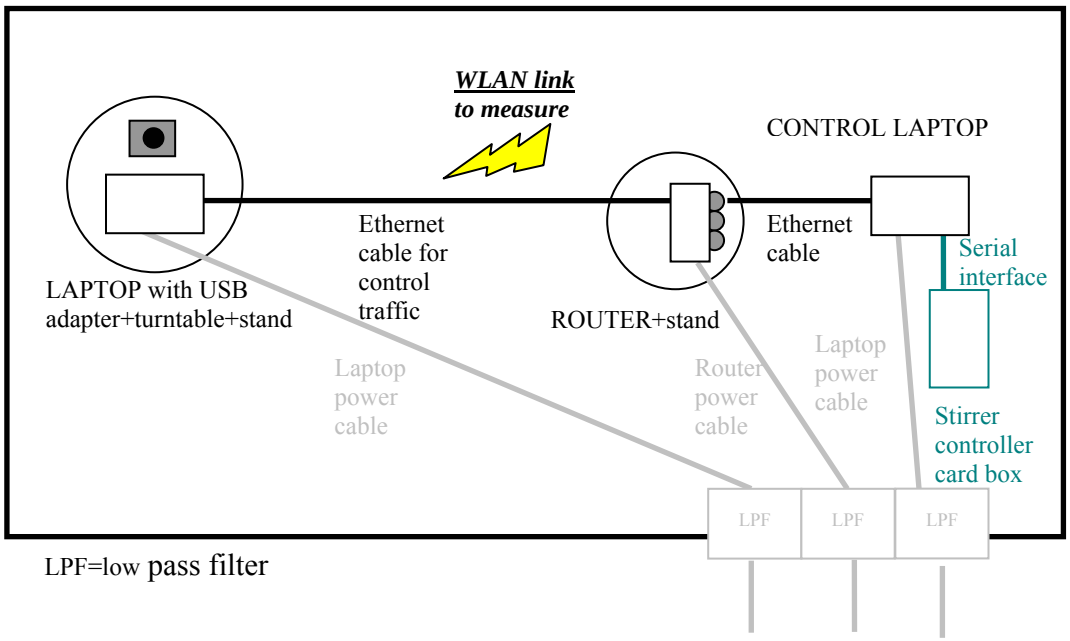

Figure 35: Improved setup layout

Traffic generator software: IxChariot, a commercial test tool with advanced traffic creation capabilities was chosen for the improved setup. IxChariot features a range of test scripts implementing more different protocols and tuning of more parameters than Iperf.

Its architecture requires the installation of *performance endpoints* in all the computers involved in the test, that is then coordinated by a more complex program called *console*. The test behaviour and characteristics are kept in a script file, edited in the console, that can also display the real-time results while the test is running. Because of the test execution being scripted in the program that also controls the stirring from inside the chamber, the console only needs to be used to edit the script that will be used in the measurement.

Regarding 802.11 wireless networks, it implements a Received Signal Strength Indicator (RSSI) reader, which allows recording the received power at one end of the link.

Test characteristics: The change in software allowed UDP testing using the Throughput script with an increased datagram retransmission timeout of 10 seconds (50

retransmissions spaced 200 ms) and modification of the send and receive buffers. These were set to the maximum UDP value in the receiver side (65490 bytes) and to half this value in the sender side (32700 bytes). The offered traffic rate was set to 70 Mbps. The link parameters were tuned so that the throughput was as high but also as stable as possible in a static situation, with datagram loss smaller than 1%. The size of the file to transfer was set to 1 MByte and 100 timing records were taken.

In this test setup with IxChariot, the fixed parameter is the amount of information to send and not the duration, so in different link conditions the test completion takes different times. When the throughput is around 50 Mbps the completion time is approximately 20 seconds. The implemented program to synchronize the stirring and the traffic generation allows giving a margin of time for the measurement to finish so that the stirring sequence is long enough to cover the whole test duration. It also allows running several tests one after the other without opening the door of the chamber.

The implementation of the Ixia's Throughput script states that the traffic is generated from the computer known as endpoint 1 to the computer known as endpoint 2 and that the RSSI statistics are recorded in the endpoint 2 if it belongs to an 802.11 WLAN. This means that in order to record the RSSI the test needs to be performed in the uplink. Other Ixia's test scripts, known as streaming scripts, allow measuring the RSSI at the endpoint 1, but the throughput behaviour they model was found to be less stable than the one of the specific tests for throughput measurement.

7.2.4 Problems and suggested modifications of the improved setup

The existence of the serial cable going inside the shielded box of the stirrer controller card is a flaw of the setup that has proved to shift the interference previously located in the lower part of the band due to factors external to the chamber, to channel 6 in the middle of the band where it is caused by the controller card. This situation can be verified in the measurement results.

It is important to substitute the metallic wires going into shielded enclosures by optic fiber links. At the same time, the fiber links must be designed so that they do not introduce impairments that lower the throughput.

7.3 Results acquired in the basic setup

7.3.1 Statistical characteristics of the measurement

Nine repetitions per channel of the measurement both during stepped and continuous stirring sequences were made in order to determine the reliability of the basic setup. All the result tables and calculations referred to in this section can be found in Annex III.

To state the accuracy of the measurement a confidence interval calculation is needed. Before actually calculating the confidence intervals, the data samples belonging to each measurement sequence of the ones described in 7.2.1 were subject to a normality test to check that the probability density function corresponded to a Gaussian and it proceeded to make the confidence interval using the t-student function. The test chosen was the Kolmogorov-Smirnov, implemented by the Matlab function *kstest*. When it was found that all the measurements fit the normal distribution, the 95%

confidence interval calculation was performed. The confidence interval, together with the standard deviation of the sample average of the nine measurement set assess the reliability of the measurement performed. Below is shown a table of these parameters together with a plot of the sample average of the measurement sequences.

STIRRING MODE	Channel number	**Standard deviation of measurements in the set**	**Largest 95% confidence interval in the set**
Stepped	2	5.35	5.33
	6	1.52	2.25
	13	0.84	2.85
Continuous	2	0.86	1.85
	6	1.22	1.14
	13	1.43	1.59

Table 4: Statistical characteristics of the measurement

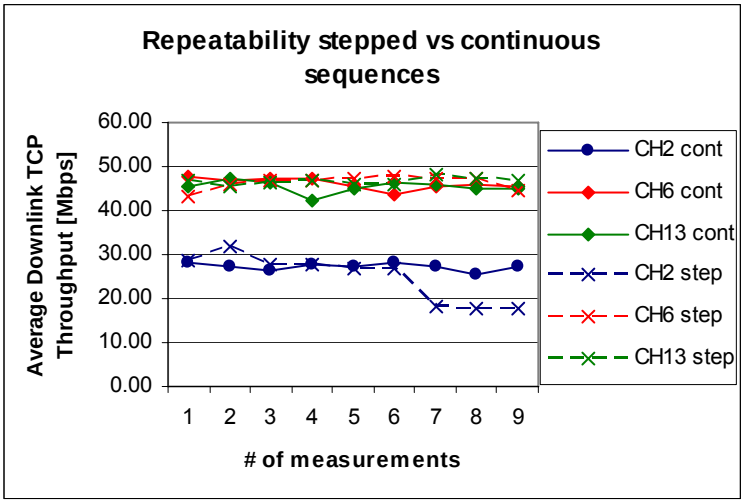

Figure 36: Repeatability of the measurement in the basic setup

This analysis shows that continuous sequences have smaller confidence intervals and standard deviation between measurements, which in turn means higher reliability and repeatability than stepped sequences. Thus it is possible to conclude that the effect of the Doppler shift induced by the stirring speed is negligible and that connection establishment in every stirrer position has a negative impact on the repeatability of the stepped measurement. TCP connection establishment takes a frame interchange of 3 segments [30], which may be complicated to carry out in a fading environment.

7.3.2 Comparison of WLAN standards

The throughput in the 802.11n MIMO 3x2 configuration was compared with the 802.11g mode of the router. For both operation modes, the modulation format was set to the most complex implemented, for 802.11n MCS 15 with 20 MHz bandwidth, that gives 130 Mbps rate MAC data and for 802.11g, 54 Mbps physical link rate. Three measurements have been taken and averaged for each of the frequency channels.

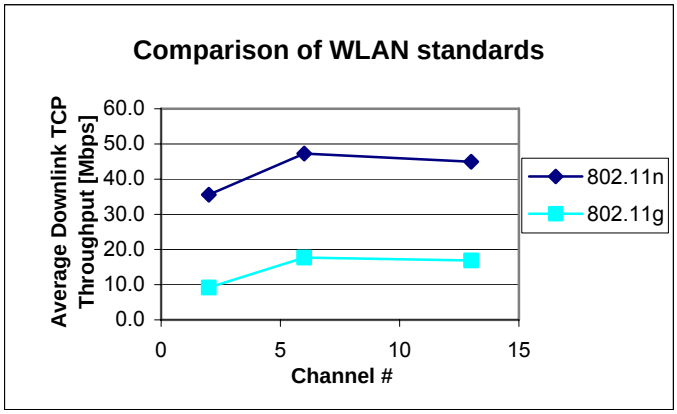

Figure 37: Comparison of WLAN standards

The comparison of WLAN standards in Figure 37 above shows how 802.11n with MIMO dramatically improves the throughput compared to 802.11g, that uses only SISO. This means an absolute increase is of at least 25 Mbps and represents on average nearly 3 times the throughput offered in the older standard.

7.4 Results acquired in the improved setup

The results shown in this stage have been acquired in the improved setup unless stated otherwise. Only three examples of measurements in the basic setup have been included for validation and comparison.

7.4.1 Average Receive Signal Strength Indicator

As described in 7.2.3, the traffic generator software IxChariot implements an RSSI reader that records the received power. Before entering the throughput considerations in the improved setup, the results for the received power in the USB adapter altering the layout of the dipole antennas in the router are presented. The antennas are fixed to the router chassis via reverse SMA connectors that allow them being removed.

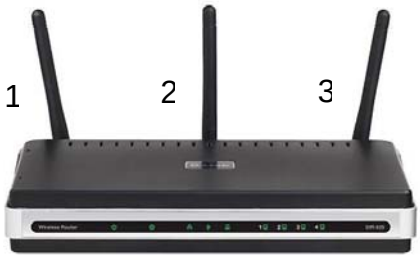

Figure 38: Antenna numbering in the router

All the possible positions removing one and two antennas were tested, measuring their average power values over a continuously stirred sequence of 100 timing records of size 1 MByte.

As a result of the implementation of the Throughput script in the IxChariot, the RSSI was recorded in the USB adapter (endpoint 1) while the transmission was in the uplink. This means the received power recorded comes from the ACKs of the router.

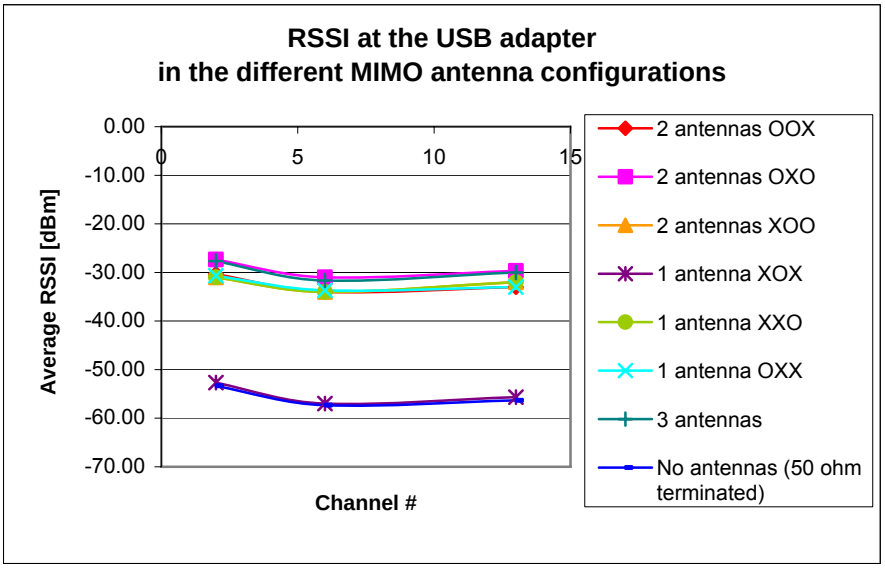

Figure 39: RSSI at the USB adapter in the different MIMO antenna configurations

Note: in the legends of MIMO configurations an X means antenna not present and an O means antenna present.

In the plot it is possible to appreciate that the received power is very similar for all the channels and slightly higher in channel 2. The figure shows that the power reading is almost identical in three cases:

CASE 1: Configurations with the three antennas or two edge antennas (*OXO*) transmitting.

CASE 2: All the rest of the two antenna configurations plus all the single antenna configurations except for the one in which only the antenna in the middle is transmitting (*XOX*).

CASE 3: The single antenna configuration with only the middle antenna and the power leakage through the router chassis when all the antennas are removed and the ports 50Ω terminated.

The following plot shows the average RSSI as a function of the antenna configuration and confirms the previous observations.

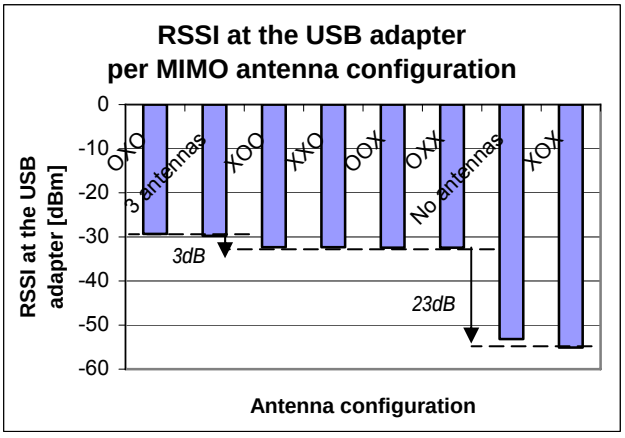

Figure 40: RSSI at the USB adapter per MIMO antenna configuration

The difference in power between the configurations allows further interpretation, when the power difference is 3dB then the received power is divided by two because there were only two antennas transmitting and one has ceased to transmit, and when the power decreases 23dB it means that there are no more antennas attached and the received power is due to the chassis leakage.

The conclusion of this measurement is that the central antenna does not transmit, perhaps because it is provided for receive diversity only. However, in the press releases to present the chipset model AR2133 by Atheros it is said that it implements a triple radio transmitter and that it can transmit over three spatially diverse channels, so there is the possibility that either the device was damaged or that the final implementation of DLINK uses only two of the antennas. More information is needed on this topic, but it was impossible to get it either from DLINK or Atheros.

On the other hand, it is possible to see that the power at each transmitting antenna is constant, but the power in the antenna system is not kept constant. There is no power redistribution when an antenna in the edge is removed, so as the antennas are removed, the transmitted power decreases.

The approach of recording the RSSI of the ACKs and then performing a loss calibration to assimilate it with the TRP of the WLAN device is the one taken by the CTIA on its "Test Plan for RF Performance Evaluation of Wi-Fi Mobile Converged Devices" [13] and could be used in the future to develop the TRP measurement in the reverberation chamber.

7.4.2 Downlink throughput of different MIMO antenna configurations

This section shows the downlink throughput values for the MIMO configurations corresponding to the previous power measurement. The MCS was set to adaptive so that the connection could be established in all the configurations.

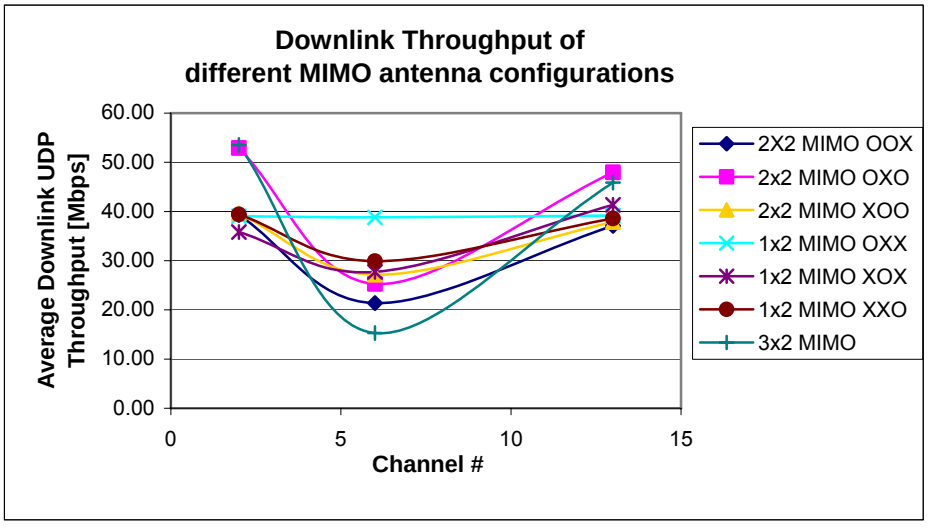

Figure 41: Downlink throughput of different MIMO antenna configurations

Note: in the legends of MIMO configurations an X means antenna not present and an O means antenna present.

The plot above shows that, for channels 2 and 13 the throughput in the original three-antenna configuration is very similar to the one where only the antenna in the middle has been removed and that all the rest of the values for one and two antenna configurations are very similar as well. This is explained by the power measurement performed before, that shows that the central antenna does not transmit. When one of the antennas in the sides is removed the case is the same as for a single transmitting antenna.

Data of two different MIMO antenna configurations are available also for the basic setup. The results correlate well with those obtained in the improved setup, configurations removing an antenna of the side mean deterioration in throughput whereas the further removal of the central antenna does not.

Nevertheless, even with a single antenna, 802.11n outperforms 802.11g, see 7.3.2, because of the improvement in the MAC features and the larger number of carriers available, as 802.11n increases the number of carriers from the 48 in 802.11g to 52. It must be noted that the measured throughput is higher in the improved setup because the transport protocol is UDP and it has less overhead and delays due to packet loss than TCP, which was the protocol used in the basic setup.

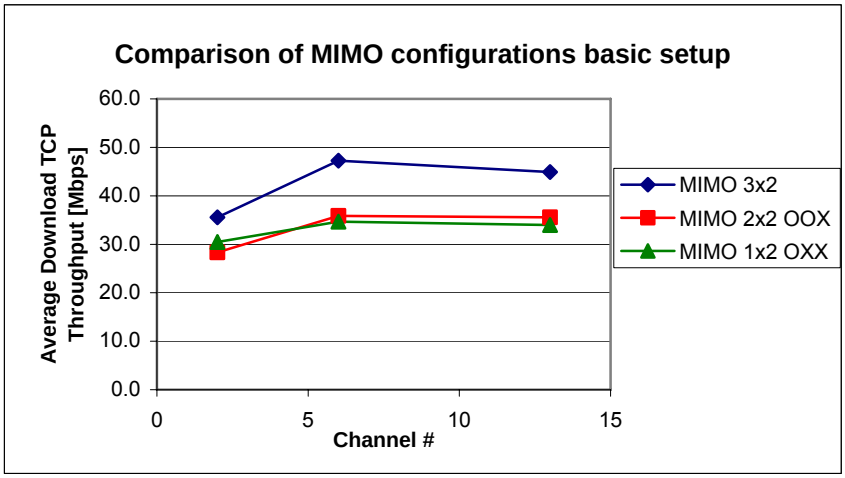

Figure 42: Comparison of MIMO antenna configurations in the basic setup

In both setups was found a frequency channel with erratic behaviour, corresponding to channel 2 in the basic setup and channel 6 in the basic setup. The fact that the wrong channel is different in the distinct setups seems to indicate that in fact both channels are working equally well in the router but there is a problem of interference in the measurement setups. The interference is located in a different frequency in each of the setups, in the basic setup the interference comes from bad isolation from the exterior due to the cables going through the chamber walls and in the improved setup the interference comes from the wire connected to the stirrer controller card.

7.4.3 Unbalanced channel cases

The case in which the antennas in a MIMO system show different performance one from the other is explored in this section. Loading the antenna ports with attenuators in an asymmetric manner, the situation in which the antennas belonging to the set have different efficiencies is mimicked. The asymmetric loading also

corresponds to a situation of fading where one of the antennas gets a weaker signal than the other, e.g. if one of the antennas is blocked by an external impediment like the head.

This was tested with the dipole set. The ports chosen to be loaded were those of the central antenna and at one of the sides of the router since the transmitting antennas are the ones in the router edges.

Apart from the awkward results of channel 6, a decrease in the throughput with the attenuation is observed in Figure 43 that is further explored in Figure 44, where the throughput results for each channel are plotted as a function of attenuation and a linear regression is performed over them. It was found that values in channel 2 and 13 accommodate well a linear dependence with the attenuation in dB (the value of R^2 is close to one in both regressions) and that the slope of the decrease is similar in both cases.

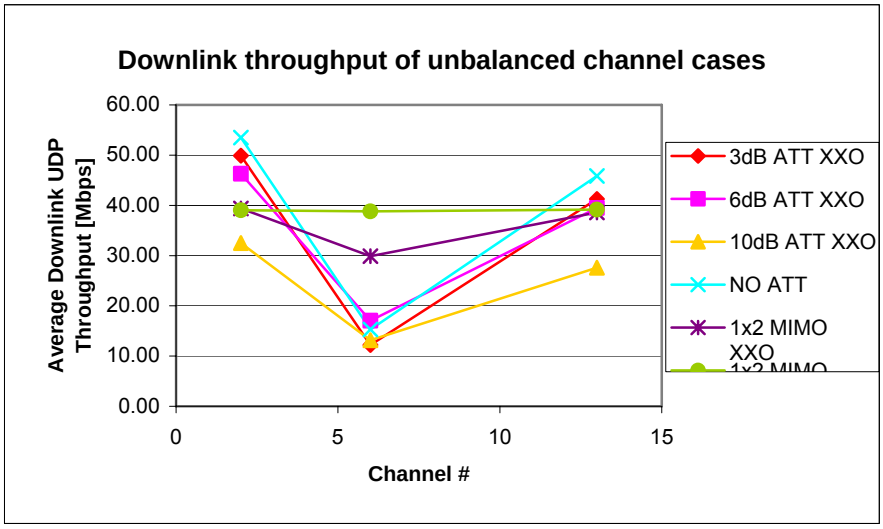

Figure 43: Downlink Throughput of Unbalanced Channel Cases

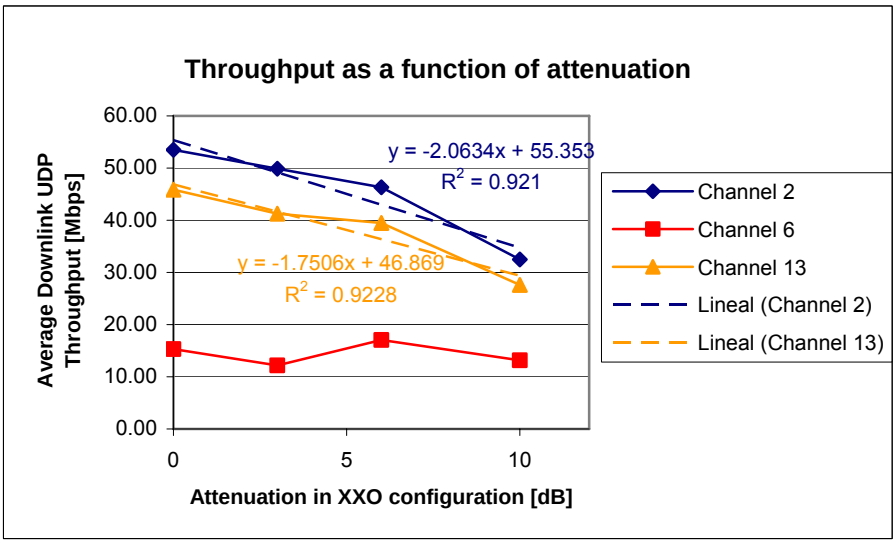

Figure 44: Throughput as a function of the attenuation in XXO configuration

The comparison between the loaded case and the single-antenna case explored in the previous section is also shown in Figure 43, that demonstrates that when there is not much attenuation in the second antenna, there is still an improvement in performance over the single antenna case. However, when the loading is above 6dB the performance is degraded compared to the single antenna case. It was found in 7.4.1 that the power allocated per antenna is constant, so the addition of an antenna will in all cases increase the transmitted power and MIMO channel capacity. The decrease of throughput under a certain loading threshold can be explained by the difficulty to separate two spatial paths of very different SNR at the signal processing of the receiver, resulting in a higher error rate and thus in a lower effective throughput than the single antenna case.

Another factor of influence regarding this question is the correlation between the spatial streams. Since the fading in the chamber is very rich, it is expected that the different signal paths are very uncorrelated and thus having a second antenna, even if it has a lower efficiency may still help to rise the throughput as long as it does not have a very low efficiency.

The conclusion is that adding a second antenna with worse efficiency enhances the throughput in a rich fading environment as long as its efficiency is not too low.

7.4.4 Downlink throughput of different MIMO antennas

The present section analyzes the impact of three different MIMO antenna sets in the router throughput respecting the three-antenna layout. Firstly the original three dipoles shipped with the router have been measured, these provide spatial diversity with an 8.5cm separation, which amounts to approximately 1.5λ at 2.45GHz. Next was a compact dielectric resonator antenna designed to be included in a portable device, that features a very small size and polarization diversity. This MIMO antenna is described in [36] and shown in the picture of Figure 45.

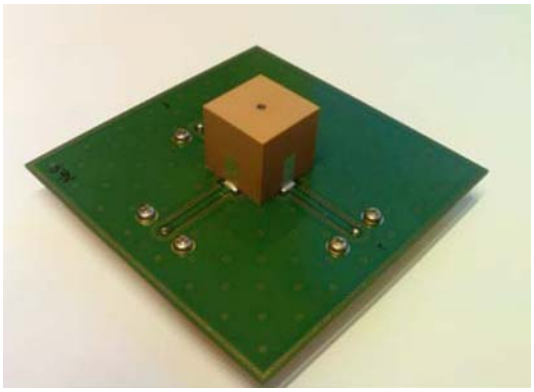

Figure 45: Dielectric resonator antenna prototype with PWB

The third MIMO antenna set was composed by the three wall antennas in the reverberation chamber. They are monopoles attached to each of the chamber walls with a very large space among them and oriented to have different polarizations, so it can be assumed that they are totally uncorrelated.

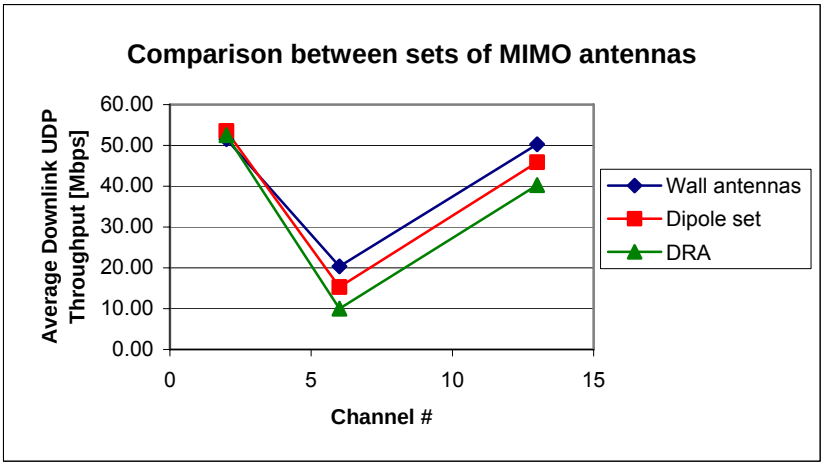

Figure 46: Downlink throughput of MIMO antenna sets

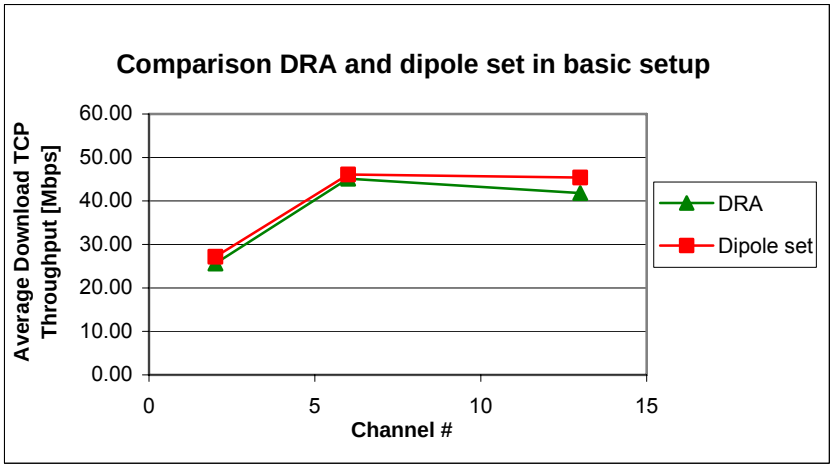

Figure 47: Comparison DRA and dipole set in the basic setup

The results show that the larger the diversity gain is for the antenna set, the higher the throughput, since the best performance is for the wall antennas, but also that it is possible to provide very high throughput in a compact device when using polarization diversity as in the MIMO dielectric resonator antenna.

The comparison between the plots of the advanced and basic setups is meaningful because it demonstrates that the dielectric resonator antenna works properly over the whole frequency band, and eventual malfunction in channels 2 and 6 comes from an external impediment.

7.4.5 Uplink throughput of different MIMO antenna configurations

Up to this stage all the measurements shown belong to the downlink, the direction of communication where the AP acts as the transmitter and the STA as the receiver. That is the direction used in applications that download data from the Internet, such as web browsing or film streaming. The measurements in this section correspond to the opposite direction of communication, the uplink. Applications like videoconference demand large throughput values in the uplink.

The first consideration regarding the uplink throughput is that the MIMO configuration is not the same as in the downlink. In the router there are two transmitting antennas but three receiving antennas, so effectively the MIMO configuration in the

downlink is 2x2 even if the three antennas are present, see 7.4.2. In the uplink the MIMO configuration is 2x3.

It is also important to point out that the output power of the adapter could not be lowered using the standard drivers, whereas in the router the power was set to low on the control web interface.

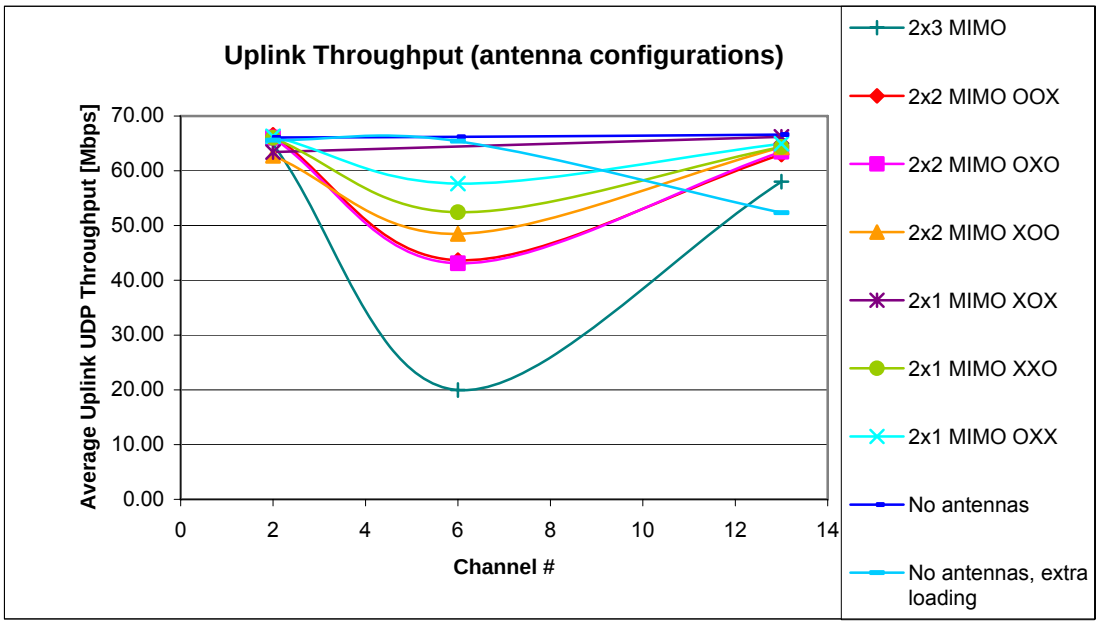

Figure 48: Uplink throughput of different MIMO antenna configurations

Note: in the legends of MIMO configurations an X means antenna not present and an O means antenna present.

The throughput values measured in the uplink are on average 12 Mbps higher than in the downlink, which means 23% improvement in performance, and do not show significant variations with the change of antenna configurations. Moreover, the system is still able to sustain this large throughput even when the antennas in the router are removed, the ports terminated, and the chamber loaded with 7 cylinders filled with lossy material. These facts are due to the large power values in the chamber, the enhanced robustness of the MIMO 2x3 configuration and the bad isolation of the receiving chains of the router.

The power margin could be reduced if a special driver allowing control of the output power of the STA, like the one available for the router, would be installed in the laptop. On the other hand, the power leakage into the receiving chains of the router could be avoided if the router chassis was set inside an isolated box and only the antennas remained out of it. This would ensure the performance in reception to be due to the antenna characteristics.

Chapter 8: Final discussion

A new setup for active measurements of throughput of MIMO systems in the reverberation chamber has been developed. The chosen communication standard was WLAN 802.11n, which has actually been the first communication standard to commercialize devices implementing MIMO. WLAN has traditionally been a computer networking standard and compared to cell phone standards presents some special features regarding its operation and characterization that were investigated. The conclusion was that for typical RF measurements with communication testers it is needed to have specific testing behaviours not included as options in the normal operation and that have to be provided by the device manufacturers as device controllers or firmware.

As much information as possible was gathered about the DUT implementation of the standard, since there are several options for operation regarding MIMO that mattered for the investigation of the test cases in the chamber. However, the lack of technical information commonly available and the denial of the manufacturers to provide these implementation details to the general public leave some aspects relatively unclear. The question of the central antenna remains unanswered, if the chipset of the router is advertised to transmit in three spatially separated streams at the time, then it is difficult to say what measurements showing no power from the central antenna mean and the impact of this fact in the developed measurement. It is needed to have a known test unit to have proper control over the measurement and reliably assess the impact of the antennas on the throughput performance.

The time-domain characterization of the reverberation chamber needs to be determined, as the characteristics of the environment are an important influence factor on the throughput measurement. It was found that for the OFDM implementation in WLAN systems the fading is slow and flat, but the possibility of generating a significant Doppler shift that impacts the BER and thus the throughput still has to be further studied. Measurement results showed that no impact of continuous stirring at the normal speed in the throughput.

Two measurement setups have been discussed and compared, with software for measurement automation that synchronizes the stirring and the throughput benchmarking developed. The measurement results showed that it is possible to get a satisfactory degree of repeatability and reliability in the measurement provided there is no interference present, with maximum and minimum values of the 95% confidence interval of a measurement of 1.85 and 1.14 Mbps and of the standard deviation in a nine measurement set of 1.43 and 0.86 Mbps respectively. The impact of interference in a shared medium technology such as WLAN was found to be determinant. There is still room for improvement of the measurement setup regarding this factor by designing a proper optic fiber link to set the computer network necessary to generate the traffic flow in a way that does not degrade the link throughput.

Some interesting WLAN cases have been studied with the developed measurement setup. Firstly the improvement of the 802.11n MIMO standard over the legacy 802.11g SISO standard was confirmed, showing an increase of three times the throughput.

By studying all the possible MIMO configurations in the router it was found that only the antennas in the edges of the device were transmitting and that the implementation of the MCS in the router makes the throughput drop by 25% when one of the antennas in the edges is removed, but shows no relevant change with the removal of the central antenna. This fact determined the loading configuration of the antennas to study the unbalanced cases to be the antenna in the centre and one antenna in the side, which yielded very good results showing the throughput decreasing linearly with the attenuation in dB.

The possibility of having a MIMO antenna set where one of the antennas is blocked by an external impediment like the head or the antennas have different efficiencies was explored by loading the antenna ports in the mentioned configuration. For the two antenna case it was discovered that when the loading is below a certain threshold there is an increase in capacity due to the second antenna, but when the efficiency is too different the throughput drops and becomes smaller than in the single antenna case. Since the power per antenna is constant in the router, this can be explained by the signal processing at the receiver not being capable of separating properly two spatial channels when their SNR is too different thus causing the BER to rise and the effective throughput to decrease. The conclusion to this matter is that a second antenna with worse efficiency enhances the performance in throughput as long as its efficiency is not too low.

A comparison of the throughput performance of three antennas with different characteristics was performed, showing on one side that antennas with more diversity gain provide better throughput on average, but on the other side that it is possible to build small antennas that yield very high throughput provided they have polarization diversity.

All the aforementioned measurements were performed in the downlink direction of communication, which is effectively a 2x2 MIMO configuration because the central antenna in the router is not transmitting. When measuring the uplink the MIMO configuration is 2x3 because the central antenna works in reception and so the performance is enhanced by 23%.

A power control issue was found when measuring in the uplink. The power margin in the chamber was so high that no difference in throughput was measured between all the MIMO configurations, and that there was no manner to cause a decrease in throughput even if the ports were terminated and the chamber loaded with very lossy material. This was due to the fact that the isolation provided by the router chassis is very poor and so as the sensitivity of the receive chains in the router must be very high, a significant amount of power can get through and sustain a very high throughput. Since the purpose of the measurement setup in the chamber is to test the antenna system, it is suggested that the router chassis should be isolated in a shielded box so that no power could be transmitted or received through the chassis and all the performance was due to the antennas.

Future work

A great deal of research on MIMO technologies can be undertaken based on the application of the presented measurement technique, such as developments of MIMO antennas, tests for different algorithm implementations regarding spatial mapping,

beamforming or channel sounding and also extension from WLAN to other communication protocols that include MIMO such as WiMAX.

Another important advantage of the reverberation chamber is that the conditions of the environment inside are flexible and can be tuned by changing the chamber load or the stirring speed. It would be interesting to evaluate the time-domain parameters of the chamber and see how they fit with existing channel models, like the ones in the TGn proposal for WLAN, and to study the limits of current stirring mechanisms to provide significant Doppler shift to different communication standards, even to introduce faster stirring with mechanical stirrers of other kinds, e.g. rotating stirrers.

It would also be possible to introduce tests to evaluate the impact of interference in throughput performance with a noise generator designed for generation of controlled impairments to communication that covered the whole transmission band.

A methodology for performance evaluation of throughput in WLAN MIMO devices in a controlled realistic environment where the original antennas are preserved has been introduced. Due to the fact that no other method has proved to be able to test the full system in such representative and repeatable conditions, it is of great interest to develop further this technique and troubleshoot issues like interference. The measurement is fast, easy to set up, and can save much time and uncertainties in comparison with current field tests, offering more reliable assessment on the performance than measurements in other shielded chambers without stirring mechanisms and measurements in channel emulators.

References

[1] LAN MAN Standards Committee of the IEEE Computer Society, “Wireless LAN Medium Access Control (MAC) and Physical Layer (PHY) Specifications”. Reaffirmed June 2003.

[2] Agilent, “MIMO Wireless LAN PHY Layer [RF] Operation & Measurement”, Application Note 1509

[3] LAN MAN Standards Committee of the IEEE Computer Society, “Wireless LAN Medium Access Control (MAC) and Physical Layer (PHY) Specifications. Higher-Speed Physical Layer Extension in the 2.4 GHz Band”. Reaffirmed June 2003.

[4] LAN MAN Standards Committee of the IEEE Computer Society, “Wireless LAN Medium Access Control (MAC) and Physical Layer (PHY) Specifications. High-speed Physical Layer in the 5 GHz Band”. Reaffirmed June 2003.

[5] LAN MAN Standards Committee of the IEEE Computer Society, “Wireless LAN Medium Access Control (MAC) and Physical Layer (PHY) Specifications. Amendment 4: Further Higher Data Rate Extension in the 2.4 GHz Band”. June 2003.

[6] LAN MAN Standards Committee of the IEEE Computer Society, “Wireless LAN Medium Access Control (MAC) and Physical Layer (PHY) Specifications. Amendment 4: Enhancements for Higher Throughput” Standard draft 3, September 2007.

[7] Agilent, “RF Testing of WLAN Products”. Application Note 1380-1

[8] CWNP Wireless Certification & Wireless Training, “Link Adaptation”, by Devin Akin]

[9] S. M. Alamouti, "*A simple transmitter diversity scheme for wireless communications*," IEEE J. Select. Areas Commun., vol. 16, pp. 1451--1458, Oct. 1998.

[10] CISCO Whitepapers, “802.11n: The Next Generation of Wireless Performance”.

[11] CTIA, “Test Plan for Mobile Station Over the Air Performance” Revision 2.2, November 2006

[12] Gregory F. Masters, “An introduction to Mobile Station Over-the-Air measurements”.

[13] CTIA, “Test Plan for RF Performance Evaluation of Wi-Fi Mobile Converged Devices” Version 1.1, August 2007

[14] IETF, RFC 1242, “Benchmarking Terminology for Network Interconnection Devices”, July 1991.

[15] “Comparison of Environments on 802.11 Throughput Performance“, Diana Lewis, Justin Rebe, and Jeremy deVries, University of New Hampshire, Interoperability Laboratory White Papers.

[16] Charles Wright, Bob Mandeville, “Clearing the Air On Wireless LAN Tests”, Azimuth Systems White Paper Collection, www.azimuthsystems.com.

[17] “Comprehensive WiMAX and Wi-Fi Product Design Demands Effective Channel Emulation”, Azimuth Systems White Paper Collection, www.azimuthsystems.com.

[18] IEEE P802.11 Wireless LANs, “TGn Channel Models”, Document IEEE 802.11-03/940r4.

[19] Atheros Communications Press Release, “Atheros Communications Expands Performance and Possibilities with First Draft 802.11n Wireless LAN Solutions”, www.atheros.com/news/xspan.

[20] Agilent, “Agilent MIMO manufacturing solution”, Application Note.
[21] Ewan Shepherd, “Addressing the new challenges of MIMO wireless LAN manufacturing test”, RF Design magazine, Oct 1, 2006.
[22] M. Bäckström, O. Lundén, and P.-S. Kildal, “Reverberation Chambers for EMC Susceptibility and Emission Analyses,” *Rev. Radio Sci. 1999–2002*, pp. 429–52.
[23] Nikolay Serafimov, Per-Simon Kildal, Thomas Bolin, “Comparison between Radiation Efficiencies of Phone Antennas and Radiated Power of Mobile Phones Measured in Anechoic Chambers and Reverberation Chamber”
[24] K. Rosengren and P.-S. Kildal, “Correlation and Capacity of MIMO Systems and Mutual Coupling, Radiation Efficiency, and Diversity Gain of Their Antennas: Simulations and Measurements in a Reverberation Chamber.
[25] K. Rosengren and P.-S. Kildal, “ Study of Distributions of Modes and Plane Waves in Reverberation Chambers for Characterization of Antennas in Multipath Environment,” *Microwave and Opt. Tech. Lett.*, vol. 30, no. 20, Sept. 2001, pp. 386–91.
[26] Martina Gabele, “Reverberation Chamber: Channel Characterization and BER measurement”, Student Research Project at Chalmers University of Technology, 2004.
[27] Hallbjörner, P.and Rydberg, A., SP Tech. Res. Inst. of Sweden, Boras. “Maximum Doppler Frequency in Reverberation Chamber with Continuously Moving Stirrer”, Antennas and Propagation Conference, 2007. LAPC 2007. Loughborough, 2-3 April 2007, pp. 229-232.
[28] T. Rappaport, “Wireless Communications Principles and Practice”, 2nd Edition, Prentice Hall, 2002.
[29] N. Geng, W. Wiesbeck, “Planungsmethoden für die Funknetzplanung”, Springer Verlag, 1998.
[30] R. Stevens, “TCP/IP Illustrated, Volume 1: The Protocols”, Addison-Wesley, 1994.
[31] Farpoint Group, “The Invisible Threat: Interference and Wireless LANs”, Document FPG 2006-321.1, October 2006
[32] P.-S. Kildal, C. Orlenius, J. Carlsson, U. Carlberg, K. Karlsson, and M. Franzén, “Designing reverberation chambers for measurements of small antennas and wireless terminals: accuracy, frequency resolution, lowest frequency of operation, loading and shielding of chamber”, EuCAP 2006, Nice, France, 6 - 10 Nov. 2006
[33] C. Orlenius, M. Franzén, P.-S. Kildal, and U. Carlberg, “Investigation of Heavily Loaded Reverberation Chamber for Testing of Wideband Wireless Units”, IEEE AP-S International Symposium, Albuquerque, N.M. 9-14 July 2006, pp. 3569 - 3572 July 2006.
[34] Iperf Version 2.0.2, Distributed Applications Support Team of the National Laboratory for Applied Network Research of the United States of America http://dast.nlanr.net/Projects/Iperf/#whatis
[35] IxChariot, Ixia, www.ixiacom.com.
[36] Katsunori Ishimiya, Zhinong Ying, Jun-ichi Takada, “A Compact MIMO DRA for 802.11n Application”, IEEE-APS, San Diego, 2008, USA.

Appendix I: Certification entities

CTIA (Cellular Telecommunications and Internet Association, www.ctia.org) is a consortium of companies of the wireless industry of the United States. It acts simultaneously as a lobby for the industry to the Congress and the Federal Communications Commission and as a certification entity to address concerns of both operators and manufacturers regarding performance of mobile stations.

IEEE (Institute of Electrical and Electronics Engineers) is an international non-profit, professional organization for the advancement of technology related to electricity.

IETF (Internet Engineering Task Force) is a large open international community of network designers, operators, vendors, and researchers concerned with the evolution of the Internet architecture and the smooth operation of the Internet. It is open to any interested individual. The IETF Mission Statement is documented in RFC 3935. The actual technical work of the IETF is done in its working groups, which are organized by topic into several areas (e.g., routing, transport, security, etc.). Much of the work is handled via mailing lists. The IETF holds meetings three times per year.

Appendix II: Router control web interface

Basic Wireless Network Settings Menu

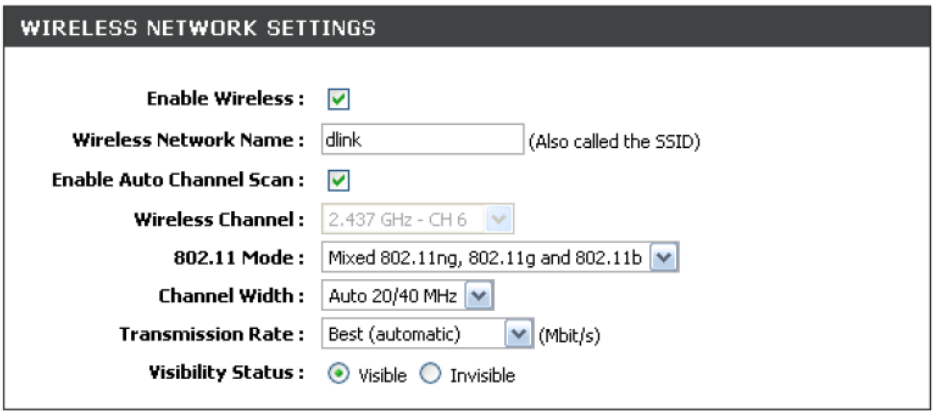

Figure 49: Wireless Network Settings Menu

Enable Wireless: Must be checked so that wireless function is on.

Wireless Network Name: Service set identifier of the wireless network.

Enable Auto Channel Scan: Allow the router to choose the channel with the least amount of interference. This disables manual channel selection.

Wireless Channel: Manual channel selection

802.11 Mode: Can be set as 802.11g Only, Mixed 802.11g and 802.11b, 802.11b Only, 802.11n Only, Mixed 802.11n, 802.11b, and 802.11g.

Channel Width: Auto 20/40 Uses 40MHz bandwidth in 802.11n unless there is a legacy device in the wireless network. 20MHz fixes the channel width to 20MHz.

Transmission Rate: Selects the transmit rate, in 802.11n devices this is paired with the MCS number. If the MCS set has a modulation format that is too complex for the SNR available no connection will be established.

Visibility Status: If the network is visible, then it is possible to find it doing a wireless networks scan at a STA. If it is not visible, then it is necessary to know the network name to connect to it because it will not be shown in the scan.

Advanced Wireless Network Settings Menu

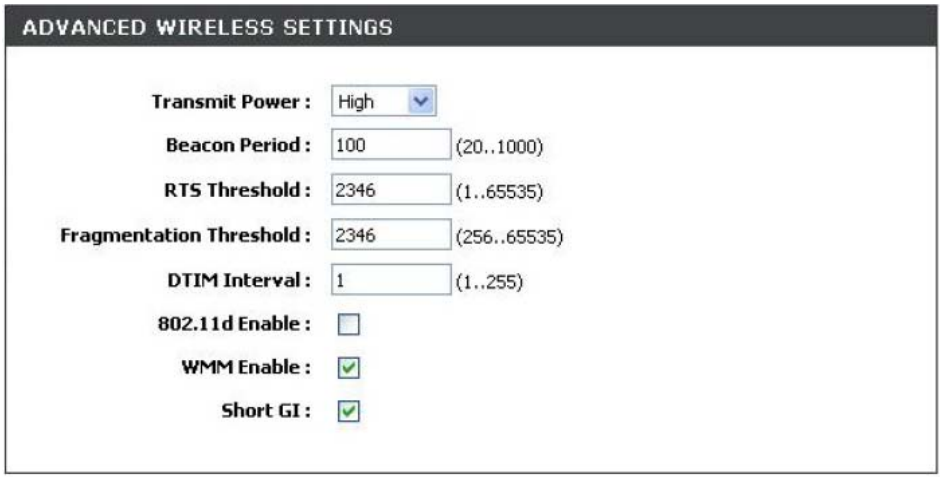

Figure 50: Advanced Wireless Settings

Transmit Power: Set the transmit power of the antennas to high, medium or low.

Beacon Period: Beacons are packets sent by an Access Point to synchronize a wireless network. 100 is the default setting and is recommended.

RTS Threshold: This value should remain at its default setting of 2432.

Fragmentation Threshold: The fragmentation threshold, specified in bytes, determines whether packets will be fragmented. Packets exceeding the size setting will be fragmented before transmission. 2346 is the default setting.

DTIM Interval: (Delivery Traffic Indication Message) countdown informing clients of the next window for listening to broadcast and multicast messages. 3 is the default setting.

802.11d: Enables 802.11d operation, a wireless specification developed to allow implementation of wireless networks in countries that cannot use the 802.11 standard. This feature should be disabled unless in one of those countries.

WMM Function: WMM is a QoS protocol for wireless networking improving the quality of video and voice applications.

Short GI: Reduce the guard interval time and therefore increase capacity.

WDS Enabled: Makes the router function as a wireless bridge with the ability to communicate with other APs.

Appendix III: Measured data used for the statistical approach

Iperf/ USB adapter only n mode							
MIMO 3x2 mcs auto bw 20/ Download							
CONTINUOUS STIRRING							
Channel	FILE#	Avg during transfer[Mbps]	Std dev during transfer[Mbps]	Peak during transfer[Mbps]	Confidence interval (a=0.05)	Avg per channel [Mbps]	Std dev between measurements [Mbps]
2	1	28.12	12.32	58.20	1.80	27.18	0.86
	2	27.12	12.41	53.30	1.81		
	3	26.28	12.66	52.70	1.85		
	4	27.62	10.96	53.20	1.60		
	5	27.14	11.43	53.00	1.67		
	6	28.27	10.99	52.60	1.61		
	7	27.12	11.15	51.20	1.63		
	8	25.52	11.48	49.20	1.68		
	9	27.41	10.44	48.00	1.52		
6	1	47.56	6.76	61.60	0.99	46.09	1.22
	2	46.77	7.79	60.40	1.14		
	3	47.19	7.43	60.30	1.08		
	4	47.10	7.00	59.20	1.02		
	5	45.51	7.52	59.10	1.10		
	6	43.61	6.78	56.90	0.99		
	7	45.51	6.06	58.20	0.89		
	8	45.95	7.35	60.80	1.07		
	9	45.61	7.48	58.10	1.09		
13	1	45.39	8.19	59.20	1.20	45.38	1.43
	2	47.09	7.01	58.70	1.02		
	3	46.45	7.40	58.90	1.08		
	4	42.15	10.88	60.40	1.59		
	5	44.89	9.55	58.70	1.39		
	6	46.38	6.69	58.50	0.98		
	7	46.04	7.48	60.20	1.09		
	8	45.02	7.71	58.10	1.13		
	9	45.00	7.94	57.30	1.16		

Iperf/ USB adapter only n mode							
MIMO 3x2 mcs auto bw 20/ Download							
STEPPED STIRRING							
Channel	FILE#	Avg during transfer[Mbps]	Std dev during transfer[Mbps]	Peak during transfer[Mbps]	Confidence interval (a=0.05)	Avg per channel [Mbps]	Std dev between measurements [Mbps]
2	1	28.58	20.68	54.29	3.02	24.84	5.35
	2	31.67	20.97	55.38	3.06		
	3	27.84	18.39	52.97	5.10		
	4	27.84	18.39	52.97	5.10		
	5	26.87	17.52	53.91	4.86		
	6	26.84	18.48	51.90	5.12		
	7	18.38	19.24	51.49	5.33		
	8	17.75	18.82	46.98	5.22		
	9	17.75	18.82	46.98	5.22		
6	1	42.97	9.04	54.27	1.32	46.27	1.52
	2	45.99	8.15	54.78	1.19		
	3	46.67	9.87	57.16	1.44		
	4	46.98	10.77	56.97	1.57		
	5	47.27	8.74	57.21	1.28		
	6	47.60	7.28	55.46	1.06		
	7	47.07	7.99	56.93	1.17		
	8	47.17	9.22	56.63	1.35		
	9	44.66	8.13	55.29	2.25		
13	1	46.91	6.69	56.03	1.86	46.58	0.84
	2	45.39	10.30	55.96	2.85		
	3	46.24	8.39	57.45	2.32		
	4	46.91	8.00	57.44	2.22		
	5	45.79	9.16	56.06	2.54		
	6	45.89	9.39	56.35	2.60		
	7	48.10	8.57	56.45	2.38		
	8	47.32	7.56	55.89	2.10		
	9	46.68	9.31	56.44	2.58		